Science of the Total Environment 409 (2011) 4387–4405

Contents lists available at ScienceDirect

Science of the Total Environment

journal homepage: www.elsevier.com/locate/scitotenv

Simulating the impacts of future land use and climate changes on surface water quality in the Des Plaines River watershed, Chicago Metropolitan Statistical Area, Illinois

Cyril O. Wilson, Qihao Weng *

Center for Urban and Environmental Change, Department of Earth & Environmental Sciences, Indiana State University, USA

ARTICLE INFO

Article history:
Received 24 March 2011
Received in revised form 25 June 2011
Accepted 1 July 2011
Available online 11 August 2011

Keywords:
Land use change
Climate change
Modeling
Water quality
Chicago Metropolis

ABSTRACT

Modeling the effects of past and current land use composition and climatic patterns on surface water quality provides valuable information for environmental and land planning. This study predicts the future impacts of urban land use and climate changes on surface water quality within Des Plaines River watershed, Illinois, between 2010 and 2030. Land Change Modeler (LCM) was used to characterize three future land use/planning scenarios. Each scenario encourages low density residential growth, normal urban growth, and commercial growth, respectively. Future climate patterns examined include the Intergovernmental Panel on Climate Change (IPCC) Special Report on Emission Scenario (SRES) B1 and A1B groups. The Soil and Water Assessment Tool (SWAT) was employed to estimate total suspended solids and phosphorus concentration generated at a 10 year interval. The predicted results indicate that for a large portion of the watershed, the concentration of total suspended solids (TSS) would be higher under B1 and A1B climate scenarios during late winter and early spring compared to the same period in 2010; while the summer period largely demonstrates a reverse trend. Model results further suggest that by 2020, phosphorus concentration would be higher during the summer under B1 climate scenario compared to 2010, and is expected to wane by 2030. The projected phosphorus concentrations during the late winter and early spring periods vary across climate and land use scenarios. The analysis also denotes that middle and high density residential development can reduce excess TSS concentration, while the establishment of dense commercial and industrial development might help ameliorate high phosphorus levels. The combined land use and climate change analysis revealed land use development schemes that can be adopted to mitigate potential future water quality impairment. This research provides important insights into possible adverse consequences on surface water quality and resources under certain climate change and land use scenarios.

1. Introduction

The spatial extent of urban areas has globally undergone dramatic growth over the past six decades (Angel et al., 2005). Within the United States, every urban area has expanded with different patterns of land use and land cover (LULC) configurations (USEPA, 2001). The dramatic alterations that humans have engineered on LULC within cities have a number of implications for terrestrial and aquatic ecosystems. Moreover, climate at regional and seasonal scales, air, and water quality have been particularly affected (Feddema et al., 2005; Foley et al., 2005; Hepinstall et al., 2008; Sala et al., 2000). As a consequence, it becomes essential to obtain an understanding of how recent trajectories of land use change will manifest in the future (Clarke et al., 1997; Rounsevell et al., 2006). This understanding is pivotal for natural resource scientists, planners, and decision makers in developing comprehensive plans for the medium to long term in tackling environmental issues (Loomis, 2002; Maestas et al., 2003; Theobald and Hobbs, 1998, 2002).

Computer simulation models have been widely engaged in estimating the likely future spatial configuration of a landscape (Theobald and Hobbs, 1998). These modeling frameworks are dichotomized into regression based and those that utilize transition potentials (Clark Labs, 2009; Clarke et al., 1997; Landis, 1993, 1995; Lee et al., 1992; Lopez et al., 2001; Parks, 1991; Petit et al., 2001; Pijanowski et al., 2002a, 2002b; Rounsevell et al., 2006; Turner, 1987; Zhang and Li, 2005). Simulation models based on regression techniques fit a relation between a number of independent variables, including population growth, land area, real estate markets, other socioeconomic variables, and their linkages to the probability of land use change (Hepinstall et al., 2008; Lee et al., 1992). The analytical modeling framework is quite simple, while the data requirement can be extensive (Wu et al., 2006). Transition potential modeling framework is underpinned by stochastic Markov-chain technique

* Corresponding author at: Center for Urban and Environmental Change, Department of Earth & Environmental Sciences, Indiana State University, Terre Haute, IN 47809, USA. Tel.: +1 812 237 2255; fax: +1 812 237 8029.
E-mail address: qweng@indstate.edu (Q. Weng).

0048-9697/$ – see front matter © 2011 Elsevier B.V. All rights reserved.
doi:10.1016/j.scitotenv.2011.07.001

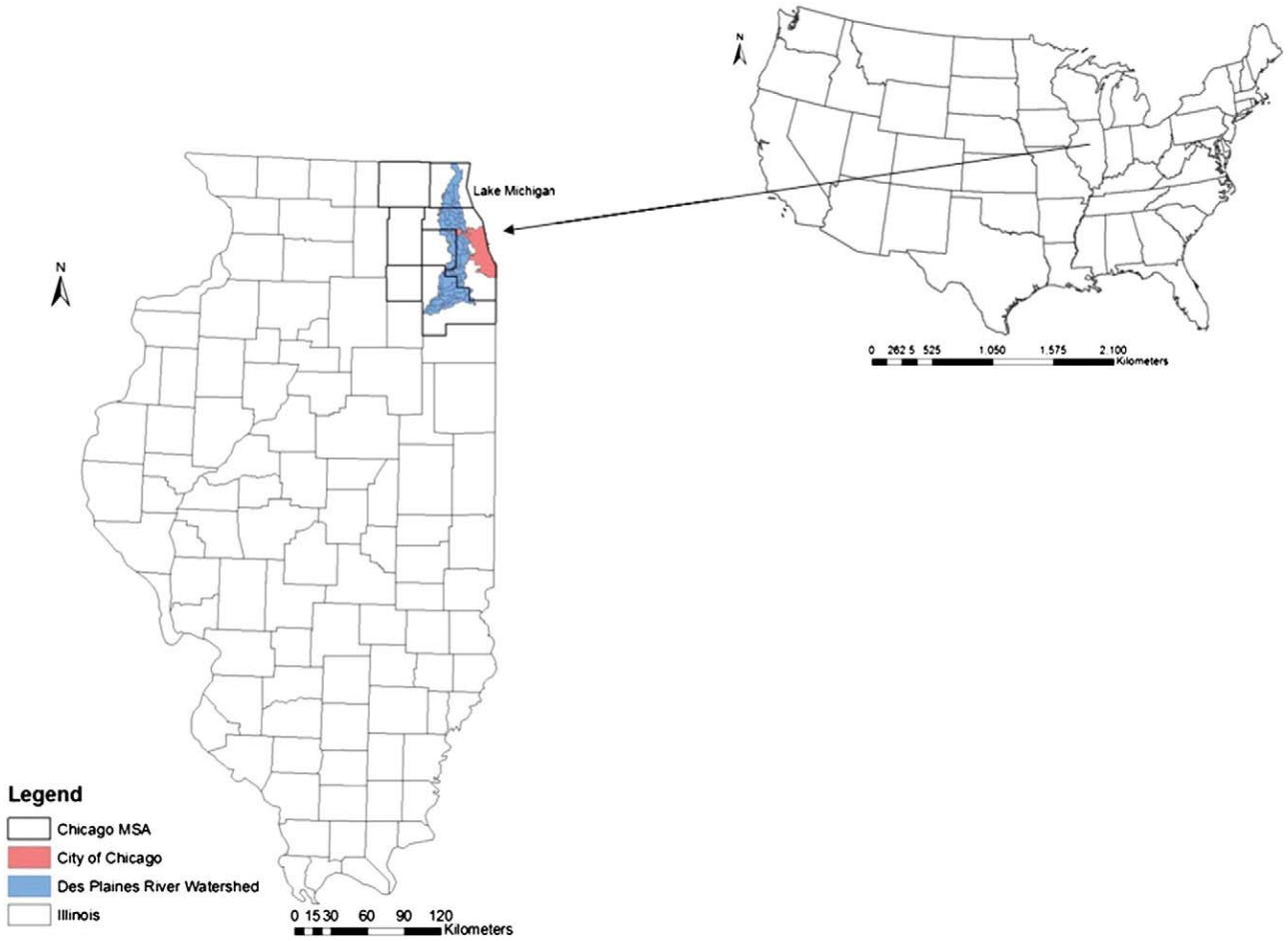

Fig. 1. Map of the U.S. showing Illinois and Chicago MSA study area.

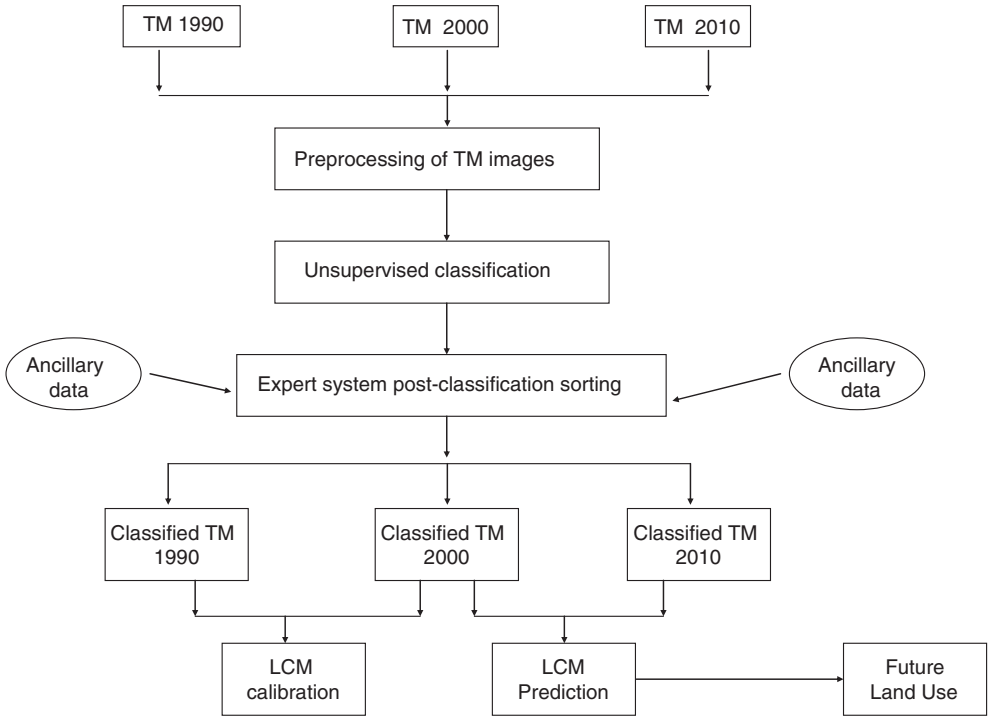

Fig. 2. Image processing flow chart and derivation of future land use images.

(Clark Labs, 2009; Wu et al., 2006; Zhou and Liebhold, 1995). A Markov chain represents a system of elements undergoing transitions from one state to a different state within a time period.

A large fraction of water quality studies explores the ramifications of historical changes in land use on surface runoff and non-point source pollution loading and/or concentration (Goonetilleke et al., 2005; Ierodiaconou et al., 2004; Lindgren, 2001; Weng, 2001; Wilson and Weng, 2010; Young et al., 1996). While an adequate amount of research has been conducted on the potential impacts of future climate changes on water resources, most of these studies did not integrate future land use configurations in their analysis (Abbaspour et al., 2009; Bekele and Knapp, 2010; Imhoff et al., 2007; Stone et al., 2001; Zhang et al., 2007). Similarly, many studies that characterized the future land use composition of an area were standalone, and did not incorporate hydrologic or water quality modeling (Clarke et al., 1997; Landis, 1995; Lee et al., 1992; Lopez et al., 2001; Parks, 1991; Petit et al., 2001; Rounsevell et al., 2006; Turner, 1987; Zhang and Li, 2005). Notwithstanding the apparent lack of integration, few studies have combined the two in analyzing the potential water quality impacts (Beighley et al., 2008; Chang, 2004; Chung et al., 2011; Ducharne et al., 2007; Maximov, 2003; Praskievicz and Chang, 2011; Tu, 2009). Responses of water quality to climate and land use changes so far remain partly understood, especially at the sub-basin level. Furthermore, most of the future land characterizations are either oversimplified, or are not directly connected to existing land cover composition when performing the forecasting. As a result, the synergistic impacts of future detailed urban land use configurations and trends, under various climate emission scenarios, on surface water quality at the sub-basin level are currently fuzzy. The main goal of this study is to provide an in-depth insight on the implications of future land use and climate change on surface water quality at the sub-watershed scale. Specific objectives include the development of three future land use/planning scenarios for the Des Plaines River watershed in the Chicago metropolitan area followed by an evaluation of the response of total suspended solids and phosphorus to the combined impacts of future land use and climate scenarios.

2. Material and methods

2.1. Study area

The study was conducted within the Chicago Metropolitan Statistical Area (MSA) located in northeastern Illinois (Fig. 1). The study examined that portion of Des Plaines River watershed that lies within the Chicago MSA. The watershed is 2055.9 km^2 and spans four counties within the Chicago MSA. The watershed lies between 41° 11′ 27.5″ and 42° 28′ 54.2″ north at the border with the state of Wisconsin, while its longitudinal expanse lies between 87° 42′ 24.1″ and 88° 15′ 28.9″ west.

The topography of the watershed is relatively flat and low in elevation. Altitude varies between 164.8 and 244.1 m above sea level. Most of the area is less than 213 m. Chicago MSA is located within the humid continental warm summer climatic region. Summers are warm and humid with an average July temperature of 23.8 °C while January temperature in winter averages around −4.2 °C; average precipitation for the region is 863 mm (Cutler, 2006). Summer is characterized by rainfall while the region receives more snow fall than rainfall during the winter period.

2.2. Land use data

Three Landsat Thematic Mapper (TM) images were used in developing future land use maps for the Des Plaines River watershed. The images were acquired by Landsat 5 satellite on June 1, 1990, May 3, 2000, and May 23, 2010, respectively. Landsat TM images are available in six reflective bands of 30 m spatial resolution. To assess the accuracy of classification of the TM images, high resolution aerial photographs, thematic topographic maps and Chicago Metropolitan Agency for Planning (CMAP) zoning maps were used (CMAP, 2010a).

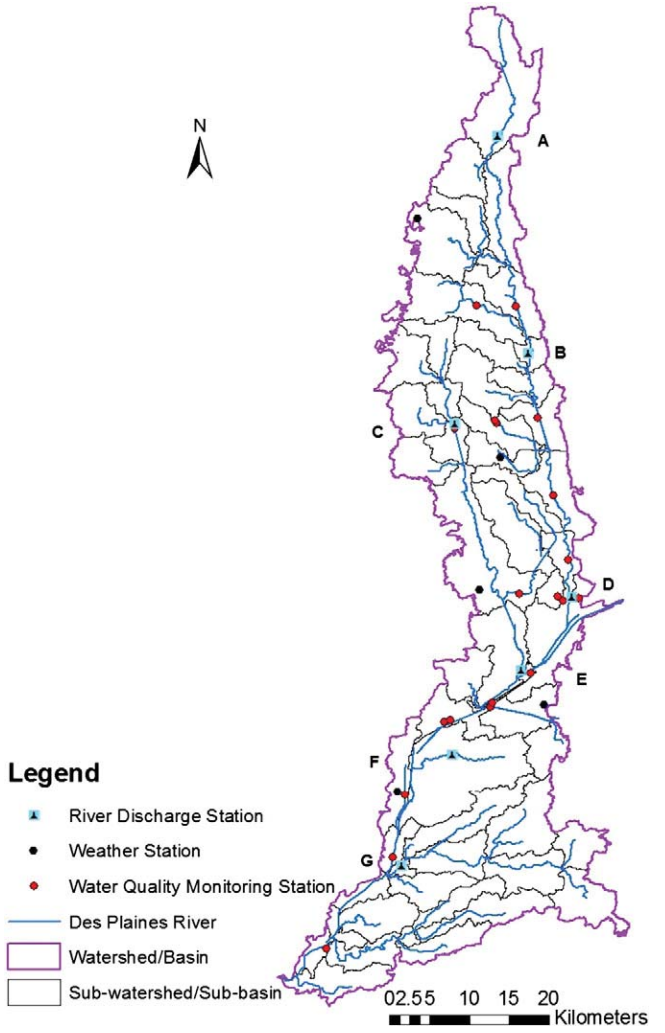

Fig. 3. Simplified SWAT model for the Des Plaines River Watershed. Note: A through G are calibrated and validated locations for flow and water quality.

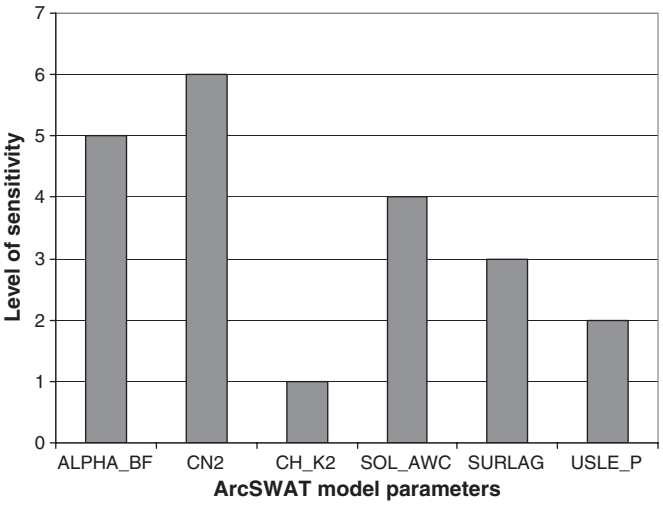

Fig. 4. Level of sensitivity of selected SWAT parameters. Note: Cn2 = Curve number for soil moisture 2. Alpha_Bf = Baseflow alpha factor. Ch_K2 = Effective hydraulic conductivity. Sol_Awc = Soil available water capacity. Surlag = Surface runoff lag time. Usle_P = Universal equation support practice factor. Level of sensitivity is dimensionless.

Table 1
Calibrated parameters of SWAT model.

Parameter	Description	Type
ALPHA_BF	Baseflow alpha factor	F
CN2	Curve number for soil moisture 2	F
CH_K2	Effective hydraulic conductivity	F
SOL_AWC	Soil available water capacity	F
SURLAG	Surface runoff lag time	F
USLE_P	Universal equation support practice factor	S
ESCO	Soil evaporation compensation factor	
PRF	Peak rate adjustment factor for sediment routing in the channel	S
SPEXP	Exponential sediment reentrained during channel sediment routing	S
FIMP	Fraction of total impervious area in urban land type	U
FCIMP	Fraction of directly connected impervious area in urban land type	U
CURBDEN	Curb length density in urban land type	U
URBCOEF	Wash-off coefficient for removal of constituents from impervious area (mm^{-1})	WQ
URBCN2	Curve number for impervious fraction	F
TNCONC	Concentration of total nitrogen in suspended solid load from impervious area (mg/N/kg sediment)	WQ
TPCONC	Concentration of total phosphorus in suspended solid load from impervious area (mg P/kg sediment)	WQ
TNO3CONC	Concentration of nitrate in suspended solid load from impervious area (mg NO3–N/kg sediment)	WQ
GW_DELAY	Ground water delay	F

Note: F = flow, S = sediment, U = urban, and WQ = water quality.

Other data used in the processing of TM images includes Digital raster graphic (DRG) images, and United States Decennial Census population and housing unit data at the block group level for 1990 and the block level for 2000.

2.3. Watershed and climate data

The Department of Agriculture Natural Resource Conservation Service (NRCS) Soil Survey Geographic (SSURGO) data provided soil data. Elevation data was solicited from United States Geological Survey (USGS) 10 m Digital Elevation Model (DEM). Climate data include National Environmental Satellite Data and Information Service (NESDIS) rainfall, snow water equivalent, and temperature data for 2006 through 2010, while future temperature and precipitation data were obtained from the Engineering Department at the University of Santa Clara at www.engr.scu.edu/~emaurer/global_data/. This spatially downscaled climate data is based on global climate model output of the World Climate Research Program's (WCRP's) Coupled Model Intercomparison Project phase 3 (CMIP3) multi-model dataset (Meehl et al., 2007). The data is available in a spatially downscaled format as described by Maurer et al. (2009) using the bias-correction/spatial downscaling method (Wood et al., 2004) to a 0.5° grid, based on the 1950–1999 gridded observations of Adam and Lettenmaier (2003). Continuous stream flow and monthly grab samples of water quality data that spans 2006 to 2010 were obtained from USGS archival station discharge data and Metropolitan Water Reclamation District of Greater Chicago water quality data respectively.

2.4. Landsat image processing and derivation of future land use maps

Landsat TM images were corrected for geometric distortion by first order polynomial method using nearest neighbor algorithm. The images were then corrected for atmospheric interference with the use of dark-object subtraction method (Jensen, 2005; Lu et al., 2002). A hybrid approach was implemented in image classification. In stage one, an unsupervised classification using Iterative Self-Organizing Data Analysis (ISODATA) classifier was employed. ISODATA classifier was used in stage one because the classification accuracy obtained from per-pixel supervised classifiers was slightly lower than that attained from ISODATA clustering. In state two, a decision tree/expert system post-classification sorting and further division of some land classes obtained during stage one of image classification was employed (Kahya et al., 2010; Lawrence and Wright, 2001; Wentz et al., 2008). Twelve land use classes were produced. Image classification accuracy ranged between 89 and 91% and exceeded the minimum threshold established for remotely sensed images (Congalton, 1991).

In developing 2020 and 2030 land use/planning scenario maps for the Des Plaines River watershed, a multiperceptron neural network built on Markov chain modeling method embedded in Idrisi's Land Change Modeler (LCM) was employed. In a Markov chain framework, the probability $p(y_t)$ that a phenomenon exists in state a_j if it was in state a_i at a previous time is denoted by the following equation:

$$p\langle y_t = a_j \,|\, y_{t-1} = a_i \rangle. \tag{1}$$

An urban landscape is characterized by various states or land use configurations which itself is dynamic through time. In modeling urban LULC over time, a number of transition probabilities have to be developed for each direction of change (Weng, 2002). This can be represented by the following Markov equation:

$$\underline{P} = \lfloor p_{ij} \rfloor = \begin{bmatrix} p_{11}, p_{12,} \cdots p_{1n} \\ p_{21}, p_{22,} \cdots p_{2n} \\ p_{n1}, p_{n2,} \cdots p_{nn} \end{bmatrix} \tag{2}$$

Where $\underline{P} = \lfloor p_{ij} \rfloor$ is the probability of transitioning from one state $_i$ to a different state $_j$ or to multiple states $(_{i1,\ i2,\ldots ij})$ as depicted by the matrix. Four drivers of land use change were included in the prediction of future land use maps for the study area. The drivers encompass evidence likelihood of change between 2000 and 2010, land value, crime level, and distance from the City of Chicago. Evidence likelihood is an empirical probability of change between an earlier land use image $(t-1)$, and a later image (t). All land use change drivers were tested for their predictive power to forecast future images. A two stage approach was adopted in developing future land use maps. The first stage used the classified land use map for 1990 and 2000 to simulate a land use map for 2010. This was done in order to ensure that the multiperceptron neural network in LCM

Table 2
Model evaluation statistics for calibration and validation of flow.

USGS stations	0552800 at Gurnee. A		0552900 at Des Plaines. B		05531500 at Western Spgs. C		05532500 at Riverside. D		0553300 at Flag Creek. E		05537500 at Lemont. F		0553900 at Hickory. G	
Statistic	Cal	Val	Cal	Val	Cal	Val	Cal	Val	Cal	Val	Cal	Val	Cal	Val
E (d)	0.68	0.69	0.79	0.82	0.84	0.78	0.83	0.75	0.71	0.74	0.64	0.60	0.62	0.69
E (m)	0.65	0.61	0.76	0.79	0.78	0.73	0.81	0.73	0.69	0.71	0.61	0.60	0.60	0.63

Note: E ≥ 0.6; (d) = daily Nash–Sutcliffe; (m) = monthly Nash–Sutcliffe; USGS = United States Geological Surveys; and E = Nash–Sutcliffe coefficient of simulation efficiency.

Table 3
Model evaluation statistics for calibration and validation of total suspended solids.

MWRDGC stations	WW 13 near USGS B		WW 17 near USGS B		WW 80 at USGS C		WW 22 near USGS D		WW 23 near USGS E		WW 29 near USGS F		WW 92 near USGS G	
Statistic	Cal	Val	Cal	Val	Cal	Val	Cal	Val	Cal	Val	Cal	Val	Cal	Val
E (m)	0.71	0.64	0.73	0.71	0.81	0.78	0.79	0.81	0.78	0.76	0.79	0.75	0.75	0.73
E_{rel} (m)	0.69	0.67	0.71	0.70	0.77	0.79	0.76	0.78	0.74	0.77	0.77	0.73	0.71	0.74
d_{rel} (m)	0.51	0.49	0.55	0.52	0.64	0.61	0.62	0.63	0.66	0.61	0.57	0.55	0.58	0.53

Note: $E \geq 0.6$; $E_{rel} \geq 0.6$; $d_{rel} \geq 0.48$; MWRDGC = Metropolitan Water Reclamation District of Greater Chicago; E_{rel} = relative Nash–Sutcliffe coefficient of simulation efficiency; and d_{rel} = relative modified index of agreement.

Table 4
Model evaluation statistics for calibration and validation of total phosphorus.

MWRDGC stations	WW 13 near USGS B		WW 17 near USGS B		WW 80 at USGS C		WW 22 near USGS D		WW 23 near USGS E		WW 29 near USGS F		WW 92 near USGS G	
Statistic	Cal	Val	Cal	Val	Cal	Val	Cal	Val	Cal	Val	Cal	Val	Cal	Val
E (m)	0.65	0.67	0.68	0.66	0.79	0.77	0.72	0.69	0.70	0.71	0.67	0.69	0.71	0.66
E_{rel} (m)	0.63	0.64	0.63	0.67	0.75	0.73	0.68	0.63	0.69	0.70	0.65	0.66	0.69	0.65
d_{rel} (m)	0.55	0.56	0.51	0.59	0.68	0.66	0.56	0.51	0.58	0.55	0.50	0.53	0.53	0.55

Note: $E \geq 0.6$; $E_{rel} \geq 0.6$; $d_{rel} \geq 0.48$; MWRDGC = Metropolitan Water Reclamation District of Greater Chicago; E_{rel} = relative Nash–Sutcliffe coefficient of simulation efficiency; and d_{rel} = relative modified index of agreement.

understood the aforementioned drivers of land use change in the watershed and also to verify the prediction of the model's land use maps. The 1990 and 2000 land use maps served as observed data for calibration of LCM while the 2010 classified land use map was used to verify the simulated map for 2010. The neural network was retrained until the simulated 2010 land use map matched with the classified map. At the completion of this exercise, the 2000 and 2010 classified land use maps were used to simulate three sets of land use maps for 2020 and 2030 respectively based on three land use/planning scenarios. In Scenario One (SN1), incentive was given to the development of low density residential and open space/vegetation land use. This was done to reflect one major goal of Chicago Metropolitan Agency for Planning (CMAP) in the 2040 Regional Plan for Chicago Metropolitan Statistical Area (CMAP, 2010b). In the second scenario (SN2), the incentive given to the growth of low density residential land class in Scenario One was removed in order to allow it to respond fully to the land use change drivers used in the study. Limited incentive was given to the development of commercial/urban land use. Incentive given to the growth of open space/vegetation was reduced compared to that established for Scenario One. In Scenario Three (SN3), higher incentive was given to the growth of commercial/urban mix land class. Slight disincentive was given to the transition of agricultural land. All other land use classes had their model parameters set to normal in order to allow them to respond to the drivers of land use change. Fig. 2 shows a schematic flow diagram of the image processing procedure and the generation of land use maps for 2020 and 2030.

Owing to the multiplicity of urban land uses and its highly dynamic nature within the Des Plaines River watershed, a total of 132 transitions took place between 2000 and 2010. Due to the multifarious land use transitions, those possessing less than 500 ha were not included in the prediction. This was done in response to the inability of LCM to process all transitions, and also to reduce the number of partial runs of the transition potential sub-model. A total of 41

Table 6
Land use change between 2010 and 2020 (%).

Land use	SN1	SN2	SN3
HD residential	−8.9	0.52	6.2
MD residential	−3.2	6.5	6.6
LD residential	10.1	8.2	9.3
Industrial	−3.5	−5.5	−5.5
TCU	2.3	2.3	2.3
Wetland	−0.8	−0.93	−0.5
Water	0	0	0
Commercial/urban mix	2.1	5.8	5.2
Institutional	0.4	0.4	0.4
Agriculture	−20.3	−24.7	−23.5
Open space/vegetation	5.5	4.6	3.9
Vacant	−1.1	−5.9	−11

Note: SN1, SN2, and SN3 = land use/planning scenarios 1, 2 and 3.

Table 5
Land use spatial extent for 2010 and 2020 (hectares).

Land use	2010	2020 SN1	2020 SN2	2020 SN3
HD residential	2868.21	2611.85	2883.26	3047.19
MD residential	26640.81	25790.42	28377.86	28406.26
LD residential	47970.72	52830.76	51921.93	52430.63
Industrial	13164.39	12698.6	12434.36	12436.93
TCU	9860.58	10093.85	10093.85	10093.85
Wetland	3723.48	3693.57	3688.68	3703.48
Water	5017.59	5017.59	5017.59	5017.59
Commercial/urban mix	13191.75	13473.71	13958.01	13890.01
Institutional	10168.56	10210.96	10209.96	10210.96
Agriculture	26890.38	21419.61	20239.82	20558.98
Open space/vegetation	32940.99	34767.1	34453.68	34221.29
Vacant	14260.32	14089.75	13418.77	12680.58
Total	206697.8	206697.8	206697.8	206697.8

Note: SN1, SN2, and SN3 = land use/planning scenarios 1, 2 and 3.

Table 7
Land use spatial extent for 2010 and 2030 (hectares).

Land use	2010	2030 SN1	2030 SN2	2030 SN3
HD residential	2868.21	2672.74	3115.04	3293.13
MD residential	26640.81	25866.12	28803.18	29235.22
LD residential	47970.72	54651.22	52163.53	53027.77
Industrial	13164.39	12508.6	12439.04	12409.36
TCU	9860.58	10113.85	10113.85	10113.85
Wetland	3723.48	3692.87	3688.68	3703.48
Water	5017.59	5017.59	5017.59	5017.59
Commercial/urban mix	13191.75	14175.71	15211.26	15029.66
Institutional	10168.56	10210.96	10210.96	10210.96
Agriculture	26890.38	21410.86	20716.61	20115.58
Open space/vegetation	32940.99	34875.74	34685.33	34019.34
Vacant	14260.32	11501.58	10532.68	10521.87
Total	206697.8	206697.8	206697.8	206697.8

Note: SN1, SN2, and SN3 = land use/planning scenarios 1, 2 and 3.

Table 8
Land use change between 2010 and 2030 (%).

Land use	SN1	SN2	SN3
HD residential	−6.8	8.6	14.8
MD residential	−2.9	8.1	9.7
LD residential	14	8.7	10.5
Industrial	−4.9	−5.5	−5.7
TCU	2.5	2.5	2.5
Wetland	−0.82	−0.93	−0.5
Water	0	0	0
Commercial/urban mix	7.4	15.3	13.9
Institutional	0.4	0.4	0.4
Agriculture	−20.4	−22.9	−25.2
Open space/vegetation	5.8	5.2	3.2
Vacant	−19.3	−26.1	−26.2

Note: SN1, SN2, and SN3 = land use/planning scenarios 1, 2 and 3.

transitions were included and executed in three separate runs, as previous attempts to include all transitions in LCM proved unsuccessful. Each transition of land use was run in separate sub-model under LCM's transition potential routine. A comprehensive land use predicted map for 2020 and 2030 was executed. At the final stage, the three comprehensive predicted maps that were generated during the forecasting exercise were combined with the use of Expert System in Erdas Imagine to arrive at one comprehensive predicted land use map for each land use scenario. This exercise was undertaken in order to capture most of the significant transitions that are likely to take place in the watershed between 2010 and the future.

2.5. Description of SWAT hydrologic and water quality model

The Soil and Water Assessment Tool (SWAT) was developed to aid the evaluation of land management practices on water supplies and nonpoint source pollution loading in watersheds and large river basins over long periods of time (Arnold et al., 1993, 1998). SWAT is an operational fully distributed model that operates on a daily time-step but can be cumulated to monthly output. The model uses a command structure to route runoff and nonpoint source pollutants through a watershed. SWAT is divided into several subcomponents which encompass hydrology, weather, sedimentation, soil temperature, crop growth, nutrients, pesticides, and agricultural management. The hydrologic sub-component can be further divided into surface hydrology and ground water hydrology. The surface hydrology routine was employed in this study. SWAT model requires numerous data which encompasses land use, soil, elevation, precipitation, temperature, humidity, stream flow, and water quality input to facilitate surface water flow and quality modeling. In this study, we employed SWAT version 2009.93.5. An extensive description of the SWAT model can be found in Arnold et al. (1998).

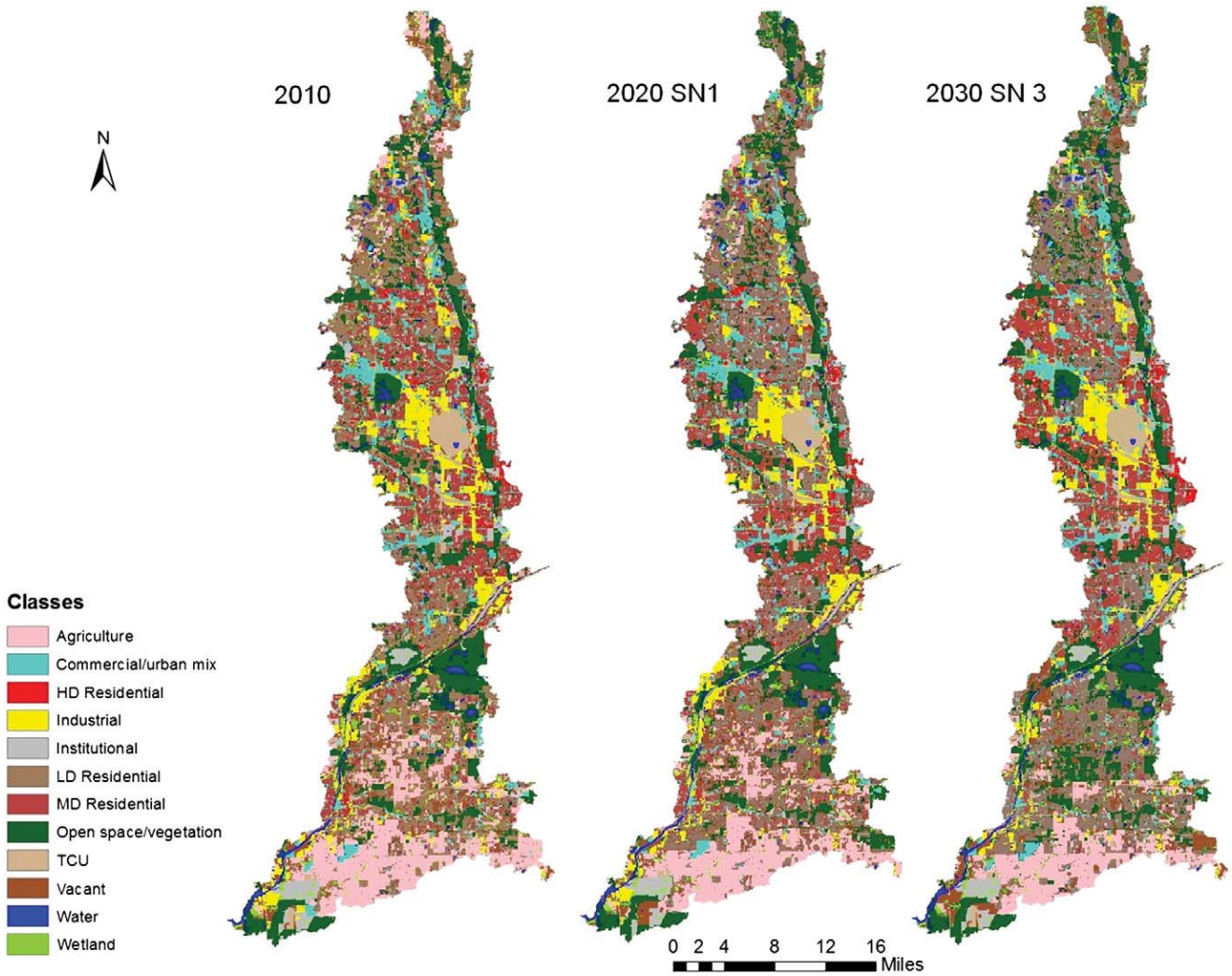

Fig. 5. Des Plaines River Watershed land use maps for 2010, 2020 and 2030. Note: HD = high density; MD = medium density, LD = low density, TCU = Transport, communication and utilities. SN1 = scenario 1, SN3 = scenario 3.

2.6. SWAT model construction

Contemporary and future climate data were spatially distributed among five weather stations within the Des Plaines River watershed (Fig. 3). These stations were selected because those outside the watershed area were too far away to influence precipitation and temperature patterns of the watershed. Future climate data that represents the Intergovernmental Panel on Climate Change (IPCC) Special Report on Emission Scenario (SRES) B1 and A1B scenarios were used in model construction and simulation. Each SRES assumes different trajectory of future economic growth and energy consumption with varying effects on the emission of green house gases and aerosol precursor (IPCC, 2001). The A1B group assumes that the world will experience rapid economic growth conditioned with the introduction of non-fossil fuel technologies that will create a balance between fossil and non-fossil energy. Whereas the B1 category envisages a world where there is a rapid change in production geared towards reduction in material intensity and the introduction of clean technologies that will replace fossil fuel energy. We employed Panoply program to visualize and extract that portion of future climate data that covers the study area (NASA, 2010). Future temperature and precipitation data were transformed before inputting into SWAT to simulating nonpoint source pollution loading for 2020 and 2030. A stochastic weather generator approach was employed to temporally downscale the average monthly WCRP CMIP spatially downscaled climate data to daily precipitation and temperature time step required by SWAT (Wilby et al., 2004; Wilks, 2010). In deriving daily future precipitation and temperature, a modified version of the chain-dependent process (a stochastic weather generator method) was employed. Following this step, the daily downscaled climate variables were summed and averaged at a monthly time step to verify its agreement with the spatially downscaled WCRP CMIP data. Areas of disagreement between the two were forced to reflect the WCRP CMIP values by simply adding and subtracting from points of under and over predictions respectively. This was implemented to avoid the problem of "over-dispersion phenomenon", wherein the variability of the two sometimes differs (Qian et al., 2008). For a detailed description of the mathematics behind the weather generator chain-dependent approach to temporal downscaling of climate variables, please refer to the works by Wilby et al. (2004) and Wilks (2010).

Seven USGS stream flow stations along the Des Plaines River were incorporated in the model to facilitate calibration and validation of flow. Twenty-two water quality stations were also included in the model to calibrate, validate, and enable comparison of water quality model results of total suspended solids and phosphorus concentrations at the sub-watershed scale (Fig. 3). Stream discharge data and water quality data spans 2006 to 2010 water years. The 2006 and 2007 data were used as 'warm up'/initializing years for the SWAT model, while the model was calibrated between 2008 and 2009, and validated for the 2010 water year. SWAT 'warm up' is essential to facilitate a fully functional model that reflects real world basin hydrology. For the 2020 and 2030 water years, model simulation started four years prior to those targeted water years in order to maintain a similar framework adopted for the 2010 water year.

A total of 13 SWAT models were independently constructed in order to effectively evaluate the impacts of land use and climate change on surface water quality. The temporal distribution of models includes one for 2010, six for 2020 and 2030 respectively. For 2020 and 2030, each model utilized the future land use/planning scenario maps under the climate variables SRES A1B and B1 scenarios. For example, each land use/planning scenario (SN1, SN2 and SN3) was modeled under future climate (B1 and A1B) emission scenarios. This approach was adopted to compare the impacts of combined land use and climate change on surface water quality. The watershed was automatically delineated with the use of a 10 meter DEM (digital elevation model) in SWAT ArcGIS extension resulting to 58 sub-basins and 1603 hydrologic response units (HRUs). A hydrologic response unit is a contiguous land area within each sub-basin that has uniform land use, soil, slope and management combination that drains directly into the sub-basin (Neitsch et al., 2004). Following model calibration and validation, final simulation runs were set up to produce mean monthly output in order to remove the biases caused by differences in daily distribution of precipitation and temperature between contemporary and future climate data.

2.7. Sensitivity analysis

Sensitivity analysis was performed on SWAT to ascertain model parameters that experienced the largest change with variations in model input. Parameters that control flow, sediment and water quality were included in the analysis. Forty-one parameters were tested for their level of sensitivity. A hybrid sensitivity analysis method that combines Latin Hypercube (LH) and One-Factor-At-a-Time (OAT) sampling algorithm was employed. Latin Hypercube allows the selection of a set of parameter values within a unique set of parameter space during each loop in the sampling process, while OAT

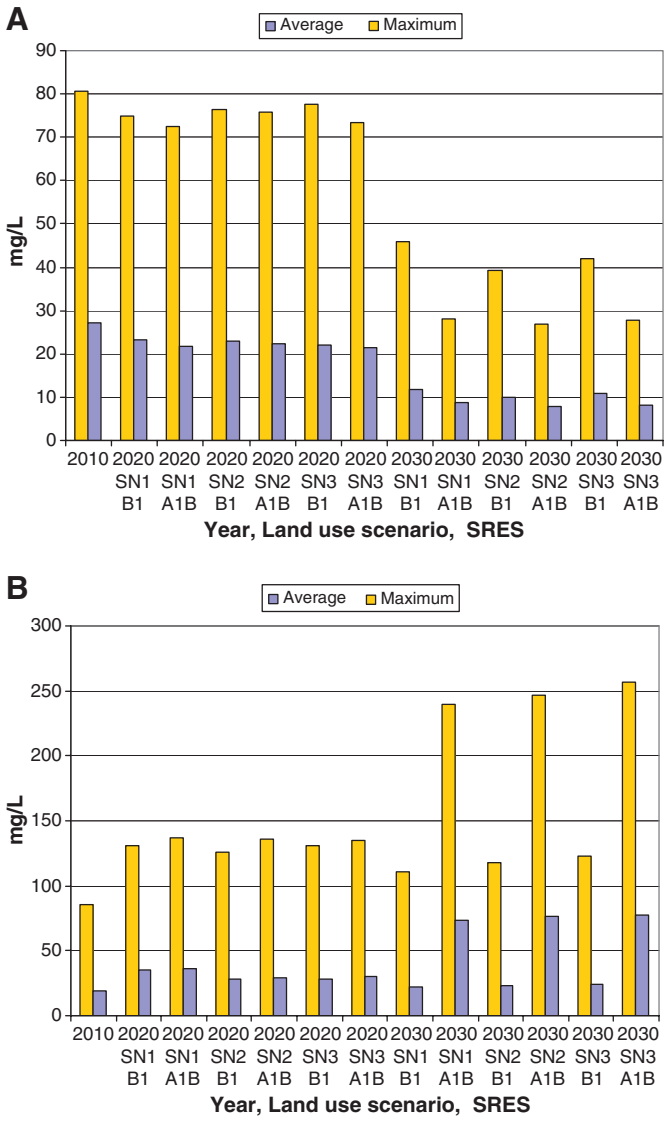

Fig. 6. Maximum and average TSS concentrations in the watershed. (A) July and (B) March. Note: TSS = total suspended solids; SRES = special report on emission scenarios; SN = land use/planning scenario.

facilitates the random selection of a parameter from each LH loop and the alteration of its value from the previous simulation by a user-defined percentage (Veith and Ghebremichael, 2009). During the sensitivity analysis, 320 simulation runs were executed. For a detailed explanation of the mechanics of the algorithm, see Van Griensven (2005). Out of the 41 parameters, 6 were ranked very sensitive and therefore given higher premium during model calibration. The relative sensitivity of the six most important SWAT model parameters for the Des Plaines River watershed between 2008 and 2010 is illustrated in Fig. 4.

2.8. Model calibration and validation

The model was automatically calibrated for flow, total suspended solids, and phosphorus. Seven model parameters were included in SWAT calibration of flow (Table 1). The model was calibrated for river flow at the sub-basin level for 2008 and 2009 water years based on daily observed river discharges at seven USGS stream discharge stations along the Des Plaines River watershed (Fig. 3). Model parameter optimization was conducted with the use of parameter solution (ParaSol) using uncertainty analysis algorithm built in SWAT-CUP software. ParaSol has its root on a modified version of the global optimization algorithm SCE-UA (Duan et al., 1993). The method uses the sum of the squares of the residuals (SSQ) as the objective function. For a detailed explanation of the model parameterization philosophy and setup, see Abbaspour (2007) and Yang et al. (2008).

At the end of auto-calibration simulation runs, an average daily Nash–Sutcliffe coefficient of 0.73 was achieved for calibration of flow from the seven stream discharge stations (Table 2). The Nash–Sutcliffe coefficient is a statistics used to ascertain whether a model is properly calibrated and validated (Nash and Sutcliffe, 1970). It is defined as

$$E = 1 - \frac{\sum_{i=1}^{n} (O_i - P_i)^2}{\sum_{i=1}^{n} \left(O_i - \overline{O}\right)^2} \quad (3)$$

where E is Nash–Sutcliffe coefficient of simulation efficiency, O_i is observed data; $\bar{O}$ is the average of observed data; P_i is simulated value, and n is the number of observations. The Nash–Sutcliffe criteria for accepting model calibration and validation were set at 0.6. Following auto-calibration, some flow parameters were manually refined to improve model simulation efficiency. SWAT was validated for flow for the 2010 water year in the seven USGS stream discharge stations mentioned above. Table 2 gives a detailed description of the efficacy of model calibration and validation of flow within the watershed.

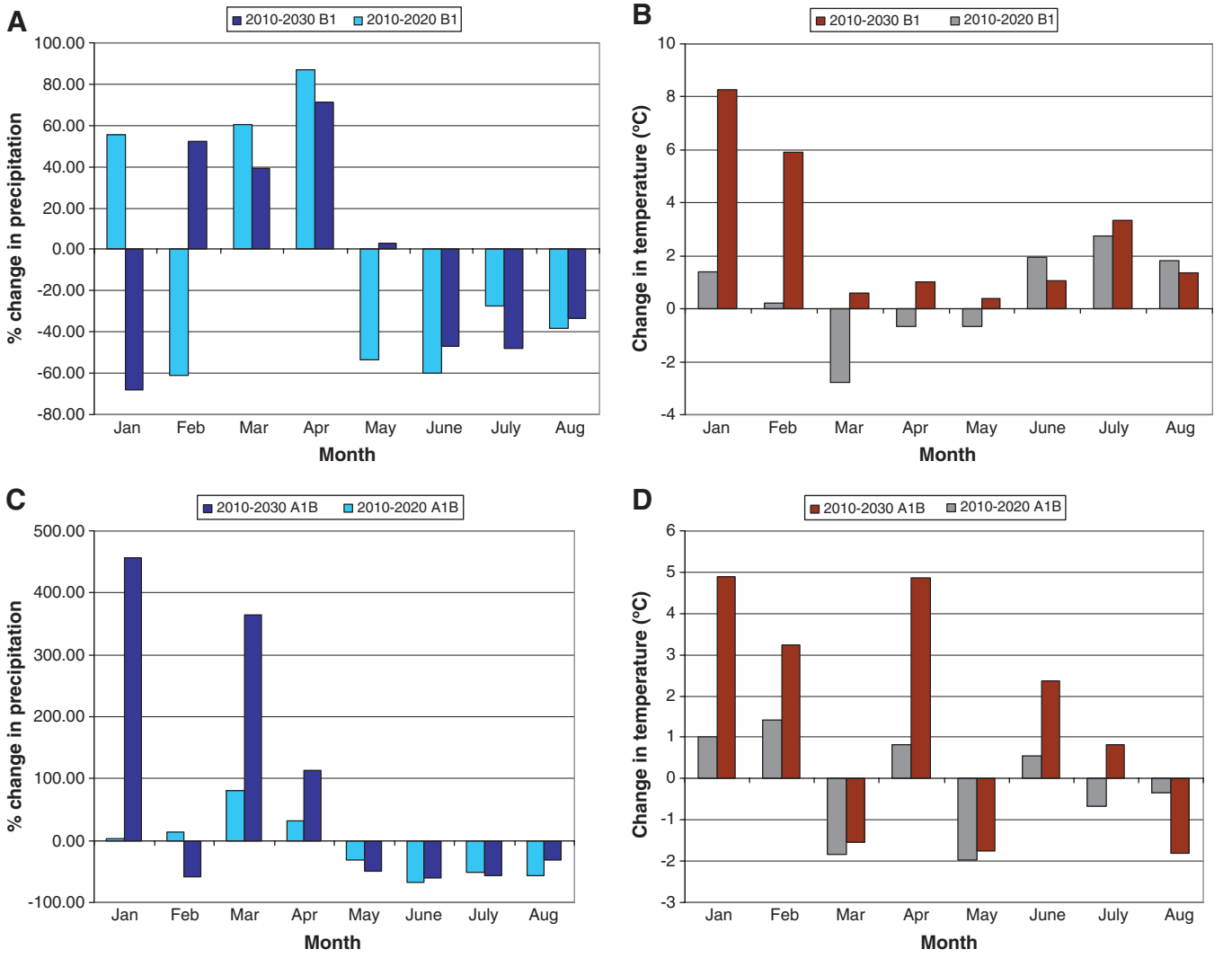

Fig. 7. Change in precipitation (A, C) and temperature (B, D) between 2010–2020 and 2010–2030.

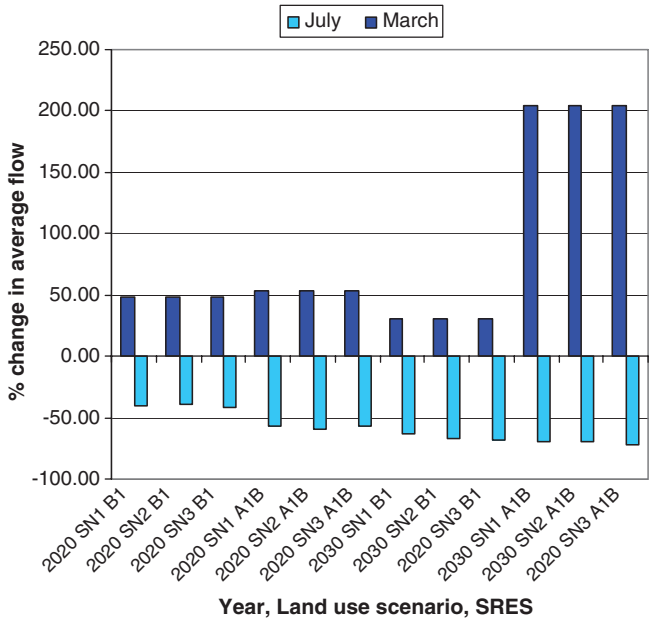

Fig. 8. Percentage change in average flow between 2010–2020 and 2010–2030.

At the completion of flow calibration, a similar but more rigorous approach was adopted in the calibration of total suspended solids and phosphorus within the watershed. The Nash–Sutcliffe relative efficiency coefficient and the relative index of agreement coefficient were also employed in assessing the efficacy of the model prediction of total suspended sediment and phosphorus concentrations (Krause et al., 2005; Willmott, 1981). Nash–Sutcliffe relative (modified) efficiency coefficient is defined by the following equation:

$$E_{rel} = 1 - \frac{\sum_{i=1}^{n} \left(\frac{O_i - P_i}{O_i} \right)^2}{\sum_{i=1}^{n} \left(\frac{O_i - \bar{O}}{\bar{O}} \right)^2} \quad (4)$$

where E_{rel} is Relative efficiency of Nash–Sutcliffe coefficient of simulation; O_i is observed data; $\bar{O}$ is the average of observed data; P_i is simulated value, and n is the number of observations. E_{rel} threshold for accepting model calibration and validation was set at 0.6. The relative (modified) index of agreement (d_{rel}) coefficient of simulation efficiency is calculated as follows:

$$d_{rel} = 1 - \frac{\sum_{i=1}^{n} \left(\frac{O_i - P_i}{O_i} \right)^2}{\sum_{i=1}^{n} \left(\frac{|P_i - \bar{O}| + |O_i - \bar{O}|}{\bar{O}} \right)^2} \quad (5)$$

where d_{rel} is relative index of agreement, O_i is observed data; $\bar{O}$ is the average of observed data; P_i is simulated value, and n is the number of observations. The relative (modified) index of agreement threshold for model calibration and validation completion was set at 0.48.

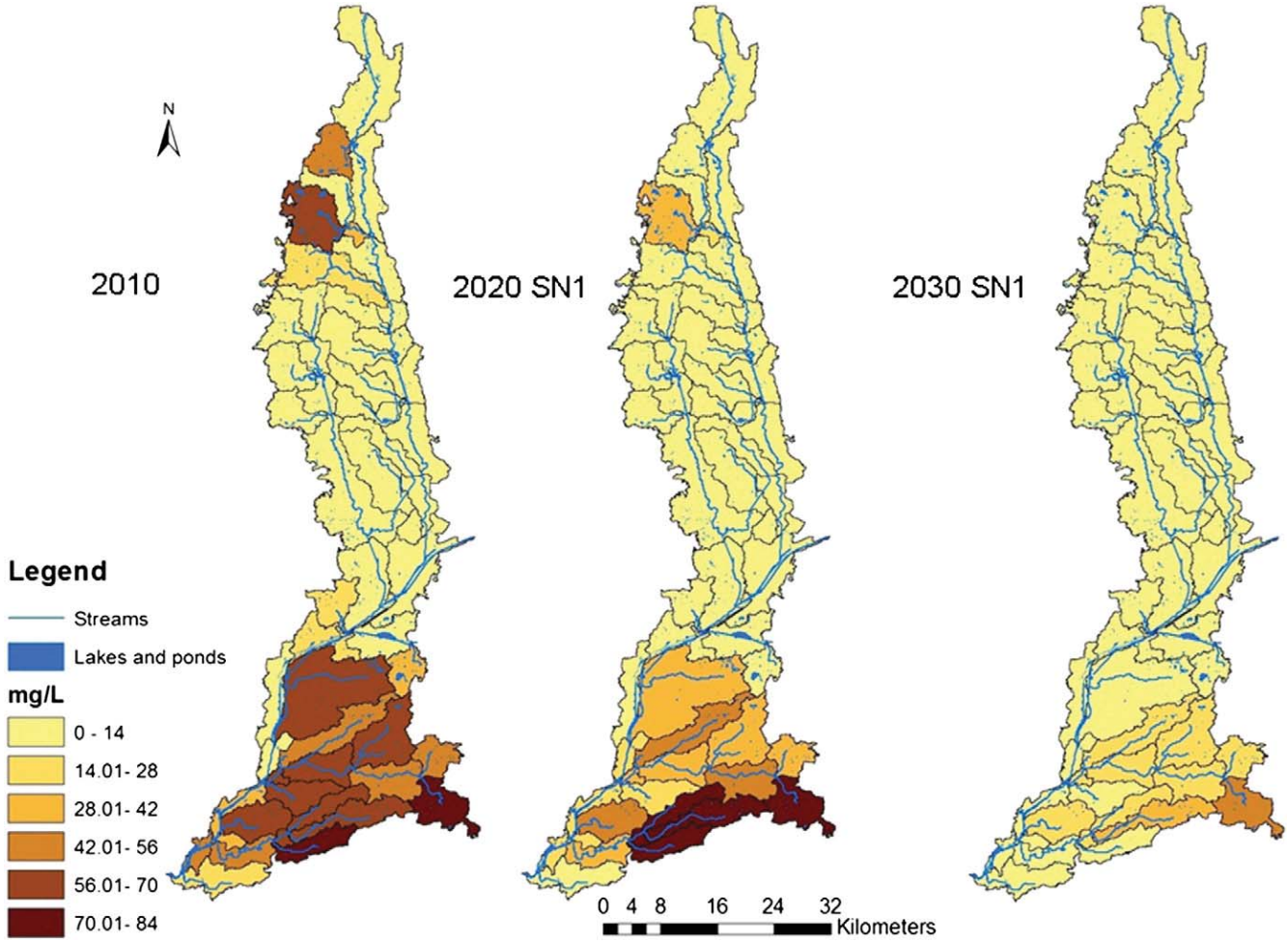

Fig. 9. Total suspended solid concentration for July under SRES B1 climate scenario. Note: SN1 = land use/planning scenario 1.

Observed water quality data were converted from concentration to load to be compatible with the units used by the SWAT model by the use of the following equation:

$$L = \int_{t_a}^{t_b} C(t) * Q(t) \quad (6)$$

where L is the 'pollutant load'(kg/d), that is transported through a specified river cross section during the time interval$\{t_a, t_b\}$, C(t) is the pollutant concentration (mg/L), and Q(t) is the river discharge in (m^3/s) at time t. Total suspended solids and phosphorus were independently calibrated for the 2008 and 2009 water years, and validated for the 2010 water year at the sub-basin scale. Seven parameters that encapsulate water quality and sediment were automatically calibrated followed by manually refining some of them. Three urban land management parameters were also manually refined (Table 1). Water quality and sediment parameters were included for calibration because sensitivity analysis pointed out that they were sensitive. Urban land management parameters were manually refined to reflect the configuration of impervious land cover in the watershed. Water quality and sediment model parameters were calibrated at a monthly time-step as a result of the lack of continuous daily water quality data. At the end of model calibration and the achievement of model simulation criteria threshold, total suspended solids and total phosphorus were validated at 7 water quality stations that are in proximate distance to the USGS stream discharge stations (Tables 3 and 4). Simulated water quality results were converted from load to concentration to make comparison with observed water quality data easier.

3. Results and discussions

3.1. Predicted land use change analysis between 2010 and the future

The Des Plaines River watershed land use maps for planning scenarios one through three (SN1, SN2, SN3) generated for 2020 estimated that the sizes of low density residential (LDR), open space/vegetation, institutional, transport, communication and utilities (TCU), commercial/urban mix, and institutional lands increased in relation to the 2010 spatial extent (Tables 5 and 6). Other land use classes that are projected to increase in some of the planning scenarios include high density residential (HDR), and medium density residential (MDR) areas. Agriculture, industrial, vacant and to a lesser extent wetlands are estimated to decrease in spatial extent by 2020 (Tables 5 and 6).

Land use change analysis between 2010 and 2030 illustrates a similar trajectory exemplified by 2020 with the exception of slight differences between spatial gains and losses among land use classes (Tables 7 and 8). For example, all residential categories demonstrated larger net gains in area by 2030 compared to that exhibited in 2020. Reduction in industrial and vacant land is more pronounced for 2030 compared to the projected value for 2020. The rest of the land covers did not show marked variation for the two future dates (Fig. 5).

3.2. Watershed response of total suspended solids to land use and climate changes

Total suspended solids (TSS) responded very differently to changes in land use and climate during the summer and winter periods of 2020 and 2030 respectively. At the general watershed level

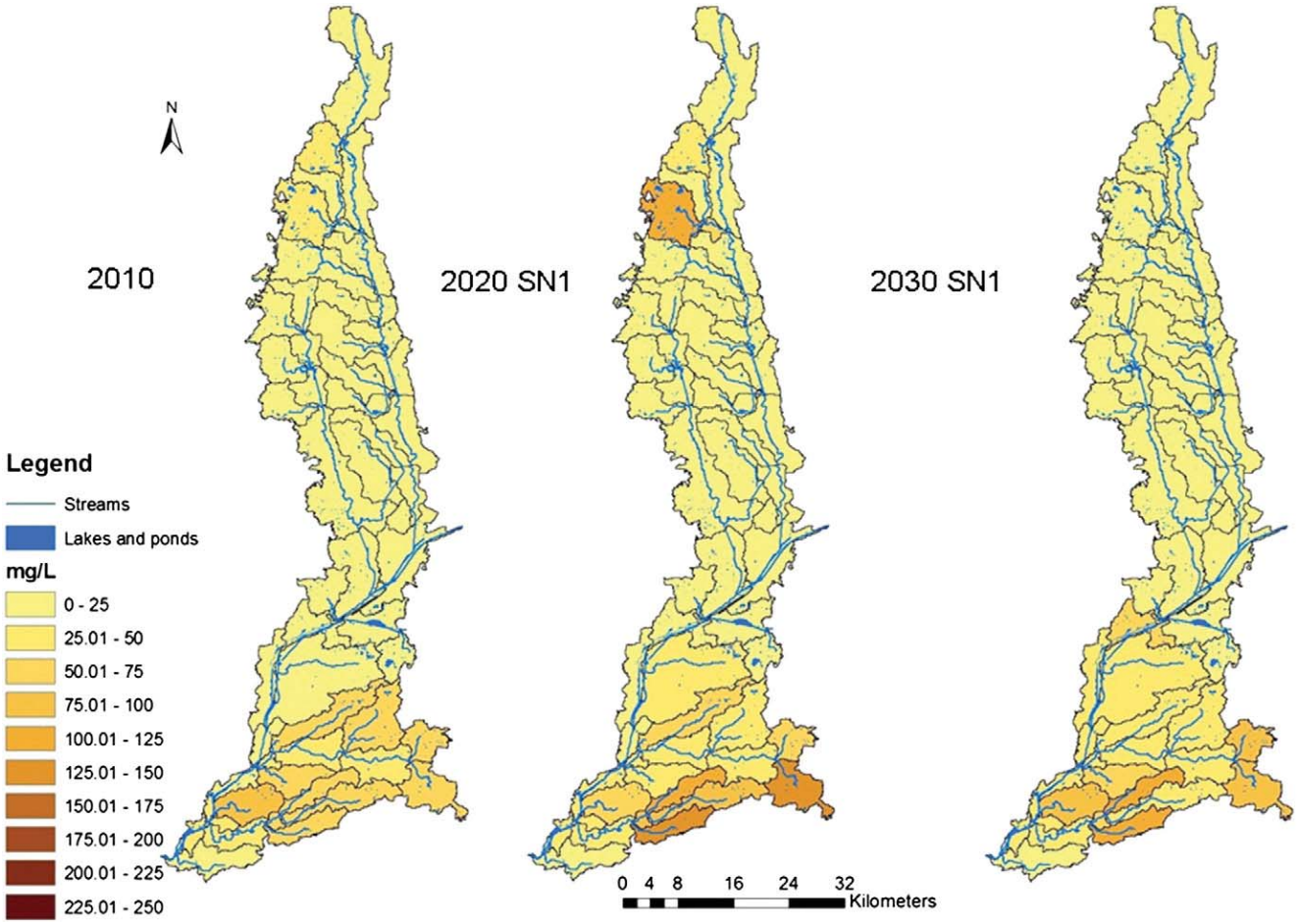

Fig. 10. Total suspended solid concentration for March under SRES B1 climate scenario. Note: SN1 = land use/planning scenario 1.

for both SRES B1 and A1B, TSS concentration was relatively higher during the month of March compared to July. These months were used to understand temporal responses of water quality to future summer and late winter/early spring climates. The difference between the average SRES B1 simulated value of total suspended solids (TSS) for July 2010 and July 2020 demonstrated a 14% decline under SN1, while the corresponding reductions for SN2 and SN3 are 16% and 19%, respectively. In a similar vein, maximum and average TSS concentrations for the month of July are predicted to wane by 2020 and 2030 for the other land use and climate scenarios compared to the baseline period (Fig. 6A). Evaluating the difference between the average SRES A1B simulated value of TSS for July 2010 and July 2020 demonstrated a 20% decline under SN1, while the values for SN2 and SN3 are 18% and 21% respectively. By July 2030, the A1B climate scenario under the three land use/planning scenarios is projected to generate the least TSS concentrations over the evaluation period.

The analysis shows that SN2 is slated to have the lowest TSS concentration over the entire study period (Fig. 6A). The inter-period decline in TSS concentration can be attributed to the dramatic estimated average reduction in precipitation and increase in temperature for July 2020 and 2030, while the differences exhibited by the various land use/planning scenarios can be ascribed to the higher reduction in agricultural and vacant lands in SN2 and SN3 (Fig. 7 and Table 6).

The maximum and average estimated TSS concentrations for March display higher values for all land use and climate scenarios compared to the baseline period (Fig. 6B). Projected increases in average TSS concentrations for March 2020 under the B1 climate scenario are slated at 78, 43 and 45% under land use/planning scenarios 1 through 3 respectively, while average TSS concentrations projected for the A1B scenarios by 2020 are slightly higher than that of B1 (Fig. 6B). Dramatic increases (>200%) in TSS concentrations are predicted for the A1B scenario by 2030, while the B1 scenario is expected to exhibit the least accretion in TSS concentration vis-à-vis the baseline period. Increment in average TSS concentration in the watershed can be attributed to increases in precipitation by 2020 and 2030. Average future precipitation for March under the B1 and A1B climate scenarios demonstrates significant increases of 60 and 365%, respectively while temperature on average displays a decline of about 2 °C compared to the baseline period (Fig. 7).

The impact of the above on TSS loading and concentration is additional erosive and transportation mechanism through higher river discharge, while lower temperatures will tend to reduce the rate of potential evapotranspiration (PET) thereby indirectly reducing infiltration rates in pervious areas of the watershed. Potential changes in river discharge between March 2010, and SRES B1 and A1B for the same month in 2020 and 2030 demonstrated an increase of between 46 and 204% respectively (Fig. 8). These inter-seasonal projected surges and abatement in TSS concentration can be attributed more to reduction and increase in precipitation during the months of July and March, respectively than the changes in the proportion of land use classes. The model results indicated greater changes in TSS concentration across climate scenarios compared to land use/planning scenarios (Fig. 6).

The general watershed response of TSS to climate and land use changes has revealed an increase in concentration levels in late winter/early spring period compared to the same season in 2010, while concentration wanes during the summer season. Studies

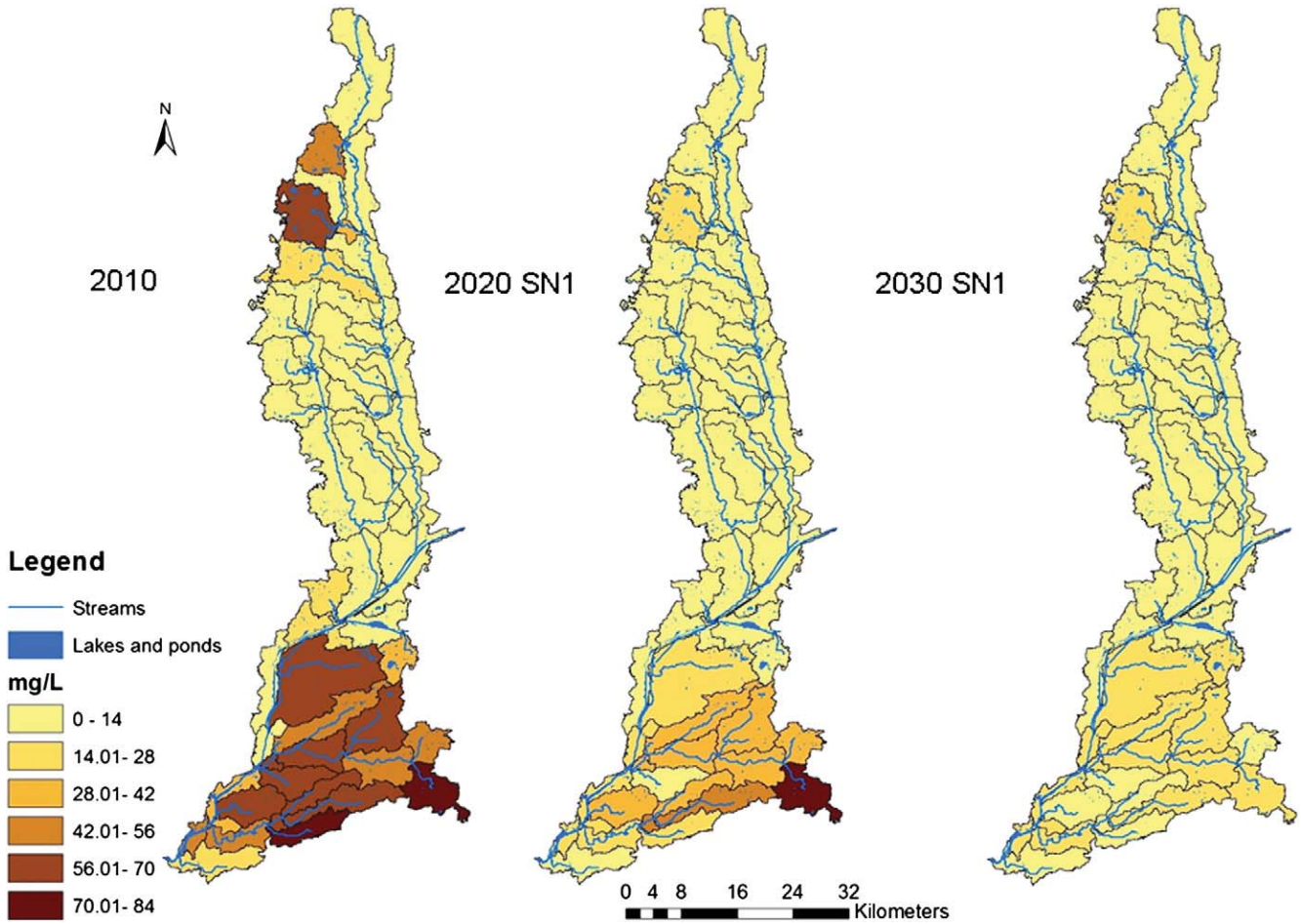

Fig. 11. Total suspended solid concentration for July under SRES A1B climate scenario. Note: SN1 = land use/planning scenario 1.

conducted on the impacts of climate change and urban development on hydrology and water quality in temperate regions have revealed higher late winter and early spring runoff compared to summer periods (Bekele and Knapp, 2010; Tu, 2009). In addition, few studies that have analyzed the response of TSS loads to climate and land use changes predicted lower loads in the summer, while the winter and early spring periods were observed to demonstrate considerable increases in loads (Asselman et al., 2003; Chang, 2004; Praskievicz and Chang, 2011). Results of this study with regard to potential TSS concentrations for water quality to a large extent are in consonance with the aforementioned scholarships. However it is problematic to make a direct comparison to these studies as their results were reported in loads rather than in concentration. Our study has revealed that TSS concentration is not always linearly related to river discharge as under certain climate scenarios, TSS concentration can be lower even though loads are projected to be higher than the baseline period. It is important that potential concentrations of constituents be calculated especially for water resource planning and management needs.

3.3. Total suspended solid response at the sub-watershed scale SRES B1

At the sub-watershed level, the model predicted that 79% of the watershed area (51 out of 58 sub-basins) will have lower TSS concentration by July 2020 under SN1, while the proportion for SN2 and SN3 are 76 and 75% respectively. Model results for 2030 predicted that 88% of the watershed area will have lower TSS concentration by July 2030, while figures for SN2 and SN3 are estimated at 83 and 84%. This differential in the spatial distribution of the pollutant between July 2020 and 2030 can be attributed to the further reduction in precipitation and runoff which was observed to affect TSS loading and concentration. Moreover, the 2030 results suggest that larger portion of the watershed area will have lower concentration of TSS concentration compared to the projected value for 2020 (Fig. 9). Average decline in TSS concentration within these sub-basins for all land use/planning scenarios over the projected period is 14.1 mg/L. General land use trend in sub-basins that are expected to have lower TSS concentrations in July 2020 compared to the baseline period encompasses an average range of decline in agricultural land (4–21%), LDR (1–12%), and slight decrease in industrial land use (1–2%), while spatial gains are demonstrated within MDR (2–8%), open space/vegetation (1–4%), commercial/urban mix (1–%), and vacant lands. Potential land use change trajectory for all the 2030 planning scenarios mirrors that demonstrated by the 2020 scenarios.

Analysis of the modeling results for March 2020 under SN1 indicates that TSS concentration will be higher in all but one sub-basin (98.3% of watershed area) compared to the 2010 values. The estimated TSS proportions for SN2 and SN3 are 98 and 100% respectively. Average increase in the pollutant is estimated at 30.5 mg/L. The general sub-basin distributional trend of TSS over the evaluation period displays an increase of the pollutant concentration within more sub-basins by March 2020 compared to the same period in 2030 (Fig. 10). The general trend of land use within areas of the watershed that is projected to have acute increase in TSS concentration by March 2020 compared to the baseline period exhibits substantial increase in LDR (6–20%), vacant (3–5%), commercial/urban mix (1–2%), slight increase in TCU, and open space/vegetation (1–4%) lands; notable reduction in MDR (>15%) is

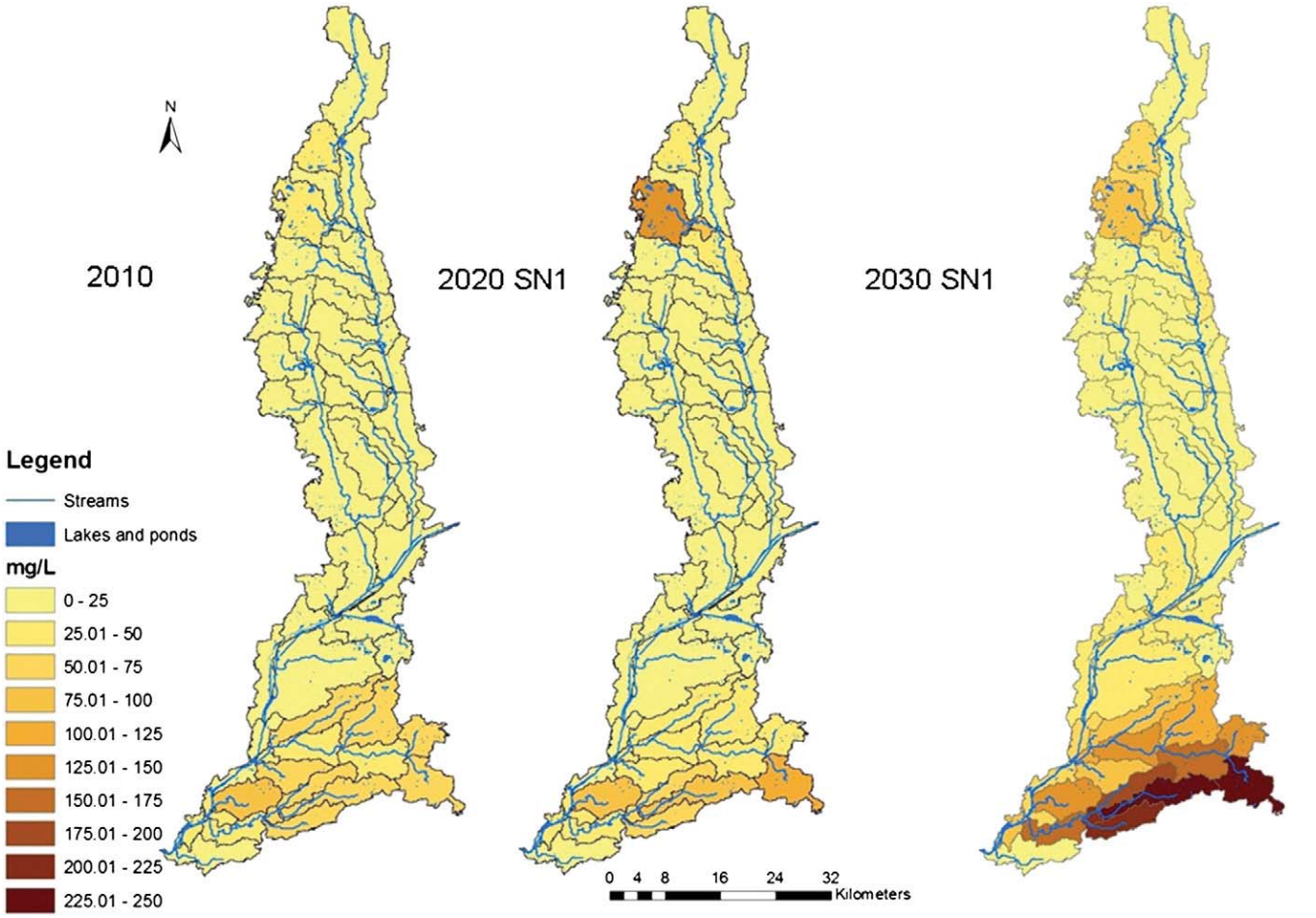

Fig. 12. Total suspended solid concentration for March under SRES A1B climate scenario. Note: SN1 = land use/planning scenario 1.

demonstrated. The other land classes did not show potential significant changes over the 20 year period.

The pattern and trend of land use displayed by the other land use/planning scenarios for 2030 are similar to that of 2020 with higher increase of additional 2 to 3% in open space/vegetation, and an inverse relationship between LDR and MDR. In some sub-basins, in both 2020 and 2030 land use/planning scenarios, there is either a large increase in LDR (20–35%) or a relatively smaller decline in MDR, or a reverse wherein MDR increase exponentially and LDR reduce at a lower rate.

3.4. Total suspended solid response at the sub-watershed scale SRES A1B

The modeling result for July predicts that between 71 and 73% of the watershed area will have lower concentration of TSS under the land use/planning scenarios for 2020, while values for 2030 are slated at 92.8% for SN1, and 87% for SN2 and SN3, respectively. Average reduction in TSS levels is projected to be higher for 2030 compared to the simulated values for all 2020 land use/planning scenarios. Fig. 11 illustrates reduction in the spatial distribution of TSS concentration between July 2010 and 2020, in addition to the projected concentrations for 2030. The pollutant is projected to continually reduce in the watershed area up to 2030. General land use trend within the sub-basins that are projected to have lower concentration of the pollutant in 2020 and 2030 under various land use/planning scenarios reveals relatively notable decline in agricultural (4–19%), LDR or MDR, and vacant (3–14%) lands, while smaller increase was observed in open space/vegetation and commercial/urban mix land classes. Land use trend mirrors that established in SRES B1 with relative imperceptible differences.

Simulation results for March 2020 demonstrate that 93, 92 and 94.7% of the watershed area will have higher TSS concentrations for SN1, SN2 and SN3 respectively in relation to the same month in 2010. The 2030 analysis predicts that 97% of the watershed area will have higher TSS concentration under SN1 and SN2, while the equivalent for SN3 is 95%. Greater numbers of sub-basins are expected to have higher concentrations of TSS by March 2030 compared to 2020 and 2010 (Fig. 12). The general land use trend within sub-basins that are expected to have higher levels of TSS demonstrates increase in agriculture (1–4%), and either high increase in LDR (7–34%) and relatively lower increase in MDR (3–8%), or vice-versa. Furthermore, marginal increase and decrease in commercial/urban mix, and industrial lands respectively are also displayed. The land use pattern and trend mirror land use scenarios under SRES B1 climate emission scenario.

The response of TSS to climate and land use changes demonstrates that the higher the precipitation level coupled with relatively low temperature, the larger the concentration of TSS in a watershed. This arises because TSS is a pollutant that responds to flushing more than dilution within a watershed and therefore, higher river discharge will mostly facilitate greater erosion and flushing/transportation of the pollutant compared to dilution (Walling and Webb, 1992; Yusop et al., 2005). The modeling results further suggest that TSS will be a major problem in most areas of the watershed during the month of March. Furthermore, the literature on historical and contemporary water quality modeling has pointed out that certain pollutants sometimes attach to suspended sediments (Bradley and Lewin, 1982; Freeman and Fox, 1995; Qu and Kelderman, 2001; Zonta et al., 2005). TSS might not only be the pollutant that will increase during the month of March but can also contribute to the transportation of other non-point source pollutants. The study has also revealed that not all sub-basins in a watershed will increased their TSS levels during periods of high river discharge in the future. The significance of this is that land use composition and slope are also important determinants of TSS concentrations within a watershed characterized by a relatively flat topography as displayed by the Des Plaines River watershed. The relatively flat topography of the watershed especially in the southern portion causes runoff to be sluggish in that zone and increase TSS load compared to the background of the water, thereby facilitating an increase in its concentration level. Analysis of TSS has also demonstrated that areas of a watershed that have middle and high density residential land are better for mitigating high levels of TSS loading during the late winter and early spring periods. Furthermore the development of a mixed land configuration wherein MDR, HDR, open space/vegetation and other land use composition are combined will augur better for TSS levels even under heavy precipitation conditions. We suggests the construction of additional reservoirs along Des Plaines River and major tributaries that can regulate excess down stream flow of water and hence reduce TSS loading at the sub-basin level during winter and early spring periods in the future. The reservoir can be structured in a way that allows normal flow of the river during the summer periods characterized by very low river discharge.

3.5. Response of phosphorus concentration to land use and climate changes

Phosphorus concentration responded differently under the climate and land use scenarios employed in this study. The model predicted that the average July total phosphorus (TP) concentration in 2020 will be higher for all land use/planning scenarios under SRES B1 compared to

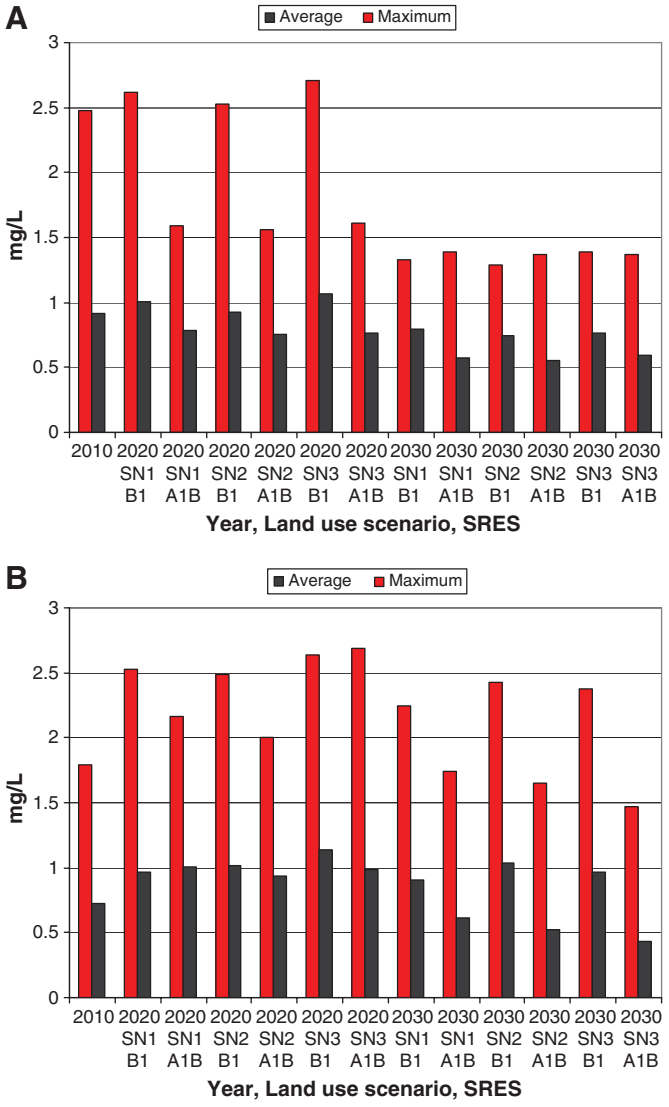

Fig. 13. Maximum and average total phosphorus concentrations in the watershed. (A) July and (B) March. Note: SRES = special report on emission scenarios; SN = land use/planning scenario.

the baseline period, while those under SRES A1B and 2030 SRES B1 demonstrated a reverse trend (Fig. 13A). The 2020 SRES B1 might have produced higher TP concentrations in July compared to the other aforementioned periods as a result of having the least reduction in precipitation (−27%) which translated to the smallest attrition in river discharge compared to the other periods in the summer (Figs. 7 and 8). Although decline in precipitation naturally reduces surface runoff and pollutant load, conversion of pollutant load to concentration revealed that the load was still higher than the background level of water, and hence concentration levels were found to be relatively higher than the other July periods. Model results suggested that by July 2030, phosphorus levels in the watershed will be lower than the estimated levels for 2020. This can be attributed to further waning of precipitation and its resultant effect on surface runoff which was found to cause lower loads compared to the background water, and hence lower concentration levels. Moreover, potential land use change analysis revealed that agricultural land, a well known source of phosphorus in watershed will significantly decline by that period (Table 8). The combination of reduced precipitation and runoff coupled with the reduction in agricultural land will most likely facilitate a reduction in phosphorus levels in the watershed by July 2030.

Analysis of model results for the late winter/early spring period demonstrated an increase in the average phosphorus level in the watershed for all land use/planning and climate scenarios with the exception of SRES A1B in 2030 (Fig. 13B). Increase in phosphorus concentrations of between 30 and 44% is estimated over the evaluation period. TP concentration is slated to be higher in the watershed in March as a result of climate related factors and to some extent potential land use changes. Analyzing changes in average precipitation and temperature between March 2010 and 2020, and also 2030, it was manifested that precipitation is slated to increase between 39 and 365% over the evaluation period; while an average drop of about −2 °C in temperature is estimated. The dramatic increase in precipitation was observed to facilitate an upsurge in river discharge. Higher river discharge and to some extent lower temperature imply that surface runoff will be increased which in turn will amplify TP loading in the watershed. The greatest increase in TP concentration is estimated for 2020 SN3 under the B1 climate scenario (Fig. 13B). Analysis of potential land use change revealed that residential areas will have the largest gains in spatial extent under SN3. Historical water quality studies have shown that expansion of urban areas tends to increase phosphorus levels in surface and ground water (Emmerth and Bayne, 1996; Waschbusch et al., 1999; Winter and Duthie, 2000). Similarly, phosphorus is attached to suspended sediments in overland flow and the increase in residential land use normally triggers high loading of suspended sediments which might translate to increase in phosphorus loading and concentration in the watershed over the study period. SWAT model result predicted lower TP concentrations for land use/planning scenarios under SRES A1B by March 2030 compared to the baseline period (Fig. 13B). Although 365% and 200% increases are estimated for precipitation and river discharge, respectively under SRES A1B by 2030, analysis of TP load revealed that load was smaller than the background level of water thereby causing significant dilution of the pollutant leading to lower concentration compared to the same month in 2010.

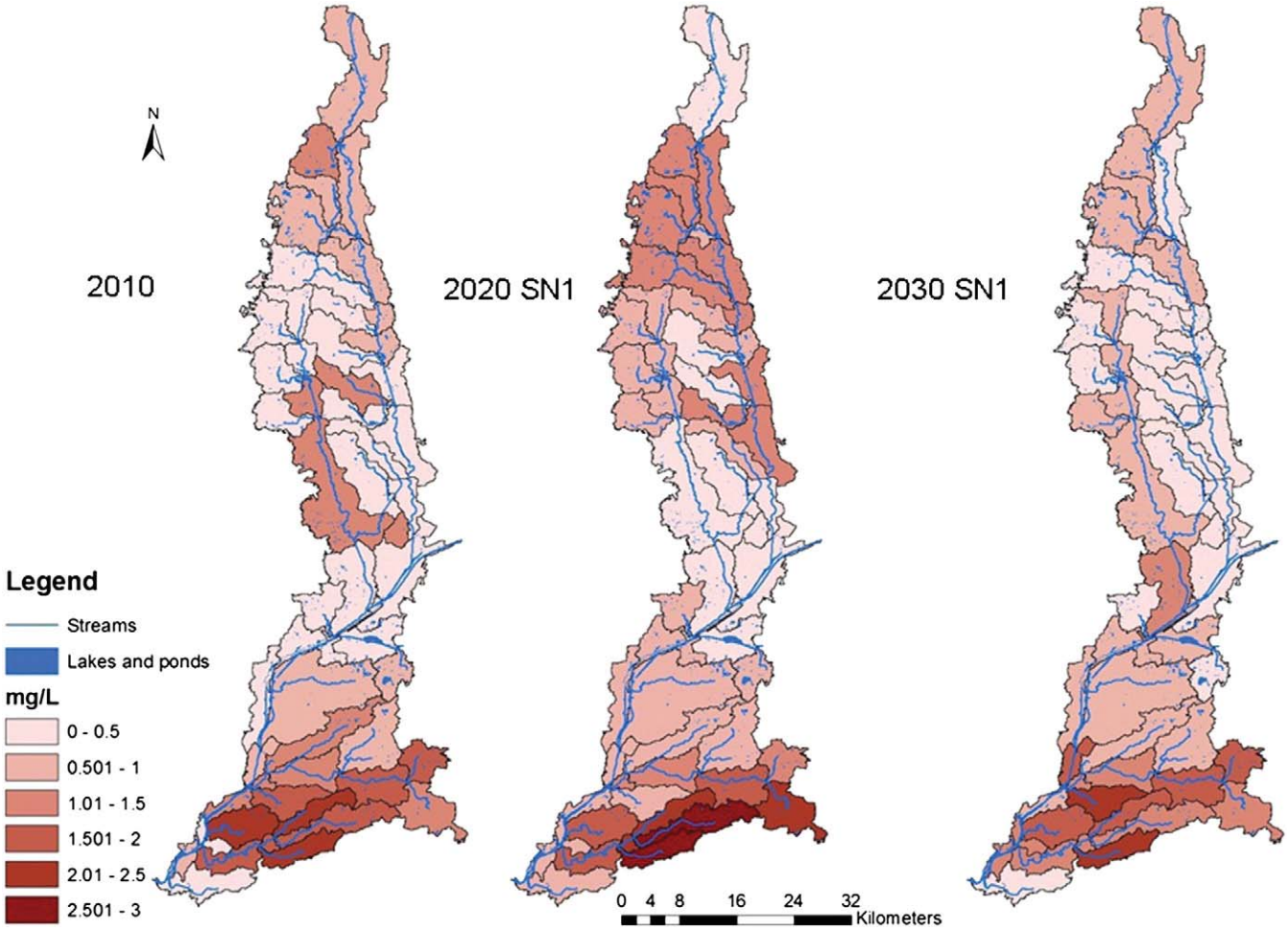

Fig. 14. Total phosphorus concentration for July under SRES B1 climate scenario. Note: SN1 = land use/planning scenario 1.

3.6. Patterns of phosphorus response at the sub-watershed scale SRES B1

The concentration of phosphorus for the month of July 2020 under SN1 through SN3 is slated to be higher in a larger portion of the watershed compared to that simulated for the same month in 2010 (Fig. 14). In SN1, the pollutant is projected to be higher in 61% of the watershed area, while projections for SN2 and SN3 are 63 and 64%% respectively. Model results for 2030 demonstrated that phosphorus concentration will be lower in a larger portion of the watershed under SN1 (62%) and SN2 (61%), while the SN3 equivalent is 54%. Land use patterns within sub-basins that are expected to have higher concentrations of phosphorus in 2020 compared to 2010 displays large areas covered with industrial, vacant, institutional, and to some extent commercial urban/mix and MDR lands. Average increase within areas of the watershed that is predicted to have higher concentration of the pollutant between July 2010 and 2020 is 0.12 mg/L. The general land use trend within these sub-basins demonstrates potential increases in MDR (3–11%), commercial/urban mix (1–4%), relatively unchanged spatial extent of industrial lands, and slight increase in open space/vegetation (2–3%) and LDR (3–9%) lands. Agricultural lands tend to decrease in most of these sub-basins and only slightly increase in few of them.

The modeling result for the month of March suggests that a larger component of the watershed will have higher concentrations of phosphorus under the various land use/planning scenarios compared to that simulated for 2010 (Fig. 15). In March 2020, it is estimated that 86, 85 and 86% of the watershed area will have higher phosphorus concentration for SN1 to SN3 respectively. An examination of phosphorus distribution for the same period in 2030 illustrates that 80, 84 and 85% of the watershed area will have higher concentrations for SN1 through SN3 respectively. Sub-basins that are expected to have elevated increase (>0.4 mg/L) in phosphorus concentration by March 2020 and 2030 exhibit land use patterns that display increase in vacant (4-7%) and LDR (8–17%), substantial increase in MDR (5–17%), modest increase in agriculture (2%), while commercial/urban mix, industrial and other land uses remained relatively unchanged.

3.7. Patterns of phosphorus response at the sub-watershed scale SRES A1B

Phosphorus concentration is projected to be lower in a large section of the watershed by July 2020 compared to the baseline period (Fig. 16). Proportion of the watershed that is projected to have lower concentration of the pollutant under the various land use/planning scenarios encompasses 65% for SN1, 66% for SN2 and 64% for SN3. An examination of the same month in 2030 demonstrates that 67% of the watershed will have lower concentration of the pollutant under SN1, while the proportion for SN2 and SN3 is 69%. Potential land use trend within sub-basins that are expected to have the greatest reduction (>0.6 mg/L) in TP concentration by 2020 and 2030 illustrates reduction in MDR (4–7%), LDR (2–7%), agriculture (2–18%) and industrial (1–3%), while open space/vegetation and commercial/urban mix exhibited increase of about 4%.

An evaluation of March results for 2020 reveals that a larger proportion of the watershed will have higher concentration of phosphorus compared to the same month in 2010, while by 2030 phosphorus concentration is estimated to dramatically reduce in the watershed area (Fig. 17). It is estimated that by 2020, TP will be higher

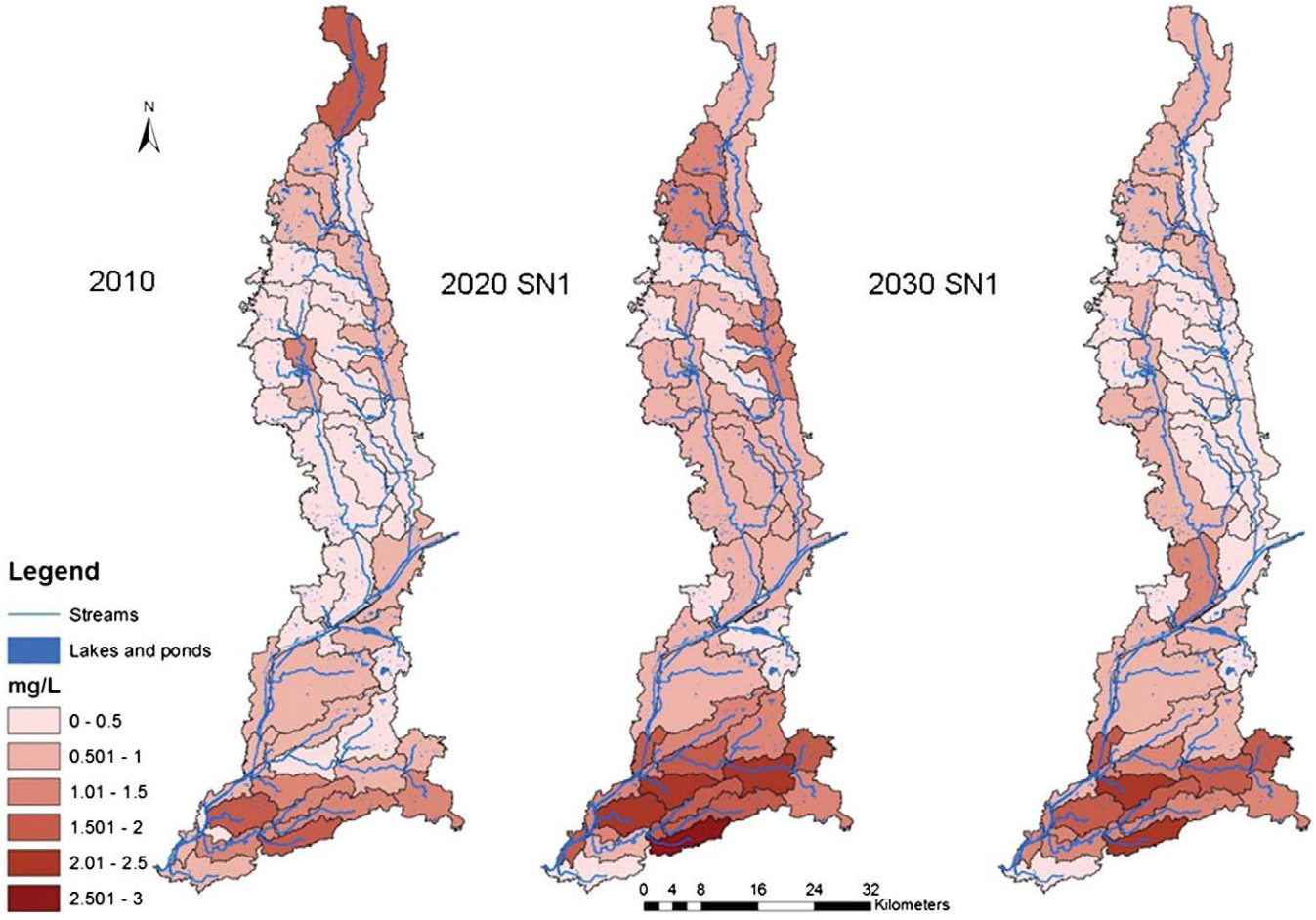

Fig. 15. Total phosphorus concentration for March under SRES B1 climate scenario. Note: SN1 = land use/planning scenario 1.

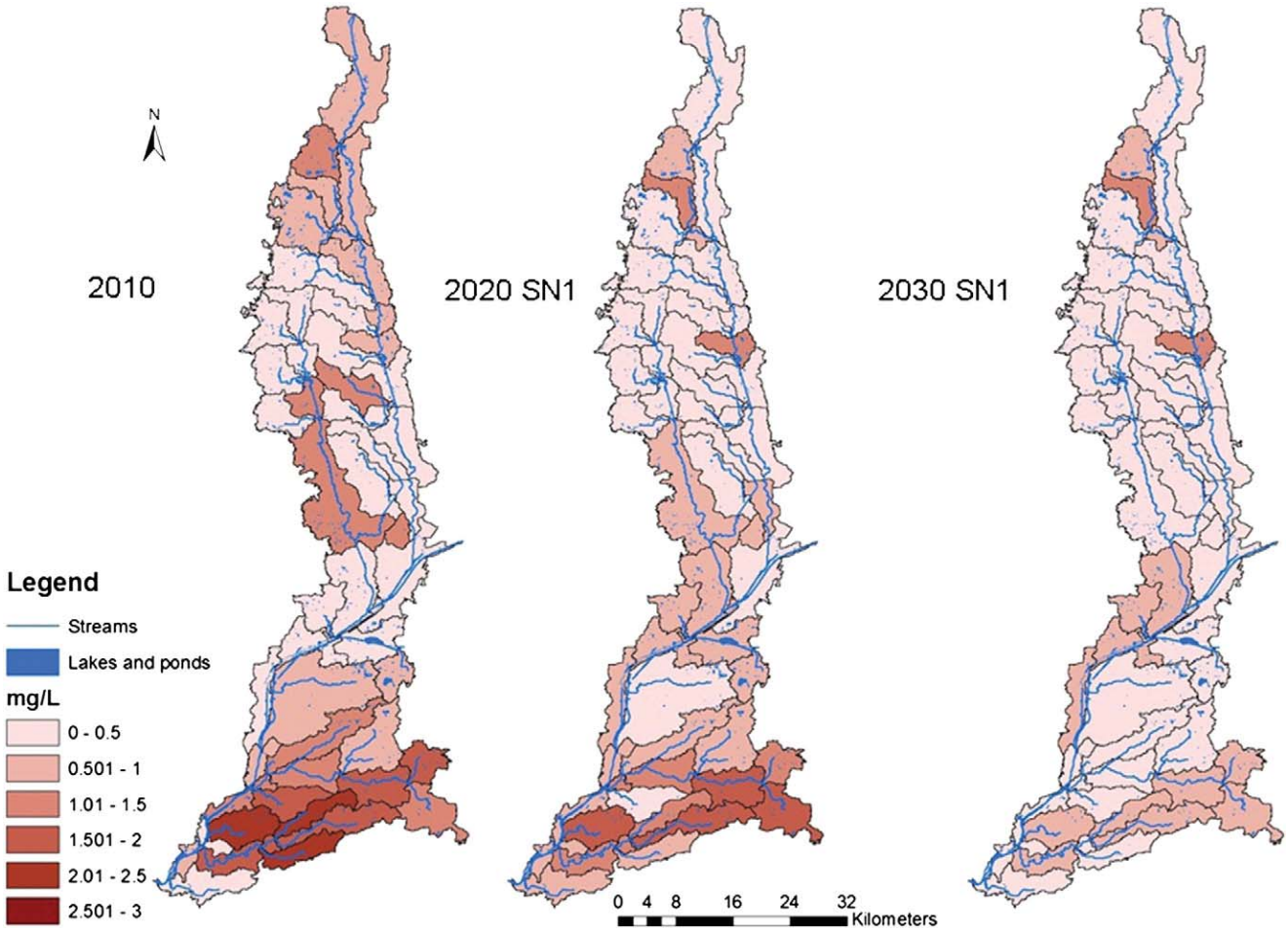

Fig. 16. Total phosphorus concentration for July under SRES A1B climate scenario. Note: SN1 = land use/planning scenario 1.

in 78, 73, and 75% of watershed area for SN1 to SN3, respectively compared to the baseline period, while by March 2030, only 40, 35, and 43% of watershed area for SN1 to SN3, respectively are slated to have higher concentration of the pollutant. Potential land use trend within sub-basins that are expected to have the greatest increase (>0.6 mg/L) in the pollutant level in 2020 demonstrated increase in LDR (3–-13%), MDR (2–7), vacant (3–7), while commercial/urban and agriculture increased at a marginal rate of less than 2%. In 2030, the larger portion of the watershed area that is expected to have lower concentration of the pollutant displays acute loss of agricultural (15–21%) land, relatively lower loss of vacant (2–7%) and industrial lands, increase in open space/vegetation (4–6%), and slight increase in MDR, LDR and commercial/urban mix land classes.

The model's prediction of a larger portion of the watershed having lower concentration of TP concentration in 2030 compared to the baseline period might have arisen out of more sub-basins being diluted as a result of the heavy runoff triggered by exponential increase in precipitation and surface runoff. Land use SN1 through SN3 under climate B1 scenario indicated that larger proportion of the watershed will have higher concentration of the pollutant in March 2030 compared to the baseline period, while under A1B, a reverse is predicted. These differences can be attributed to potential climate changes more than land use changes as demonstrated above. The behavior of TP concentrations to climate and land use changes illustrated a complex relationship when inter-period and inter-seasons are taken into cognizance. On average, summer periods demonstrated lower TP concentration levels compared to the baseline period while the winter period displayed a reverse with the exception of the A1B climate scenario for 2030. This study has revealed that potential TP especially in the late winter/early spring period will be problematic within populated areas compared to other sections of the watershed. Although previous studies have not directly examined discreet sub-basin scale land use and climate change impacts on TP loads and concentrations, some of the findings of this sub-basin scale approach to potential land use and climate change analysis can be partly related to few studies that have analyzed historical and partially projected source areas of phosphorus concentrations within watershed. Winter and Duthie (2000) concluded that phosphorus loading was found to be significant within urban land use compared to peripheral areas, while Soranno et al. (1996) predicted that future phosphorus loading within a completely urbanized watershed will be inimical to water quality. Furthermore, studies that have analyzed the impacts of climate and land use changes on phosphorus compounds have illustrated that phosphorus loading will be higher in the winter compared to the summer periods in temperate climates (Chang, 2004; Jeppesen et al., 2009; Praskievicz and Chang, 2011). The general watershed scale result of this study is in agreement with these scholarships. However, the presentation of loads as against concentration in most of these studies makes it difficult to make a direct relation of this study to the aforementioned studies as the effect of dilution under heavy precipitation and runoff regimes significantly makes the result of concentrations veer away from the linear relationship between flow and phosphorus levels in the watershed.

4. Conclusion

This study has revealed that future land use and climate changes have the potential of dramatically changing the concentration levels

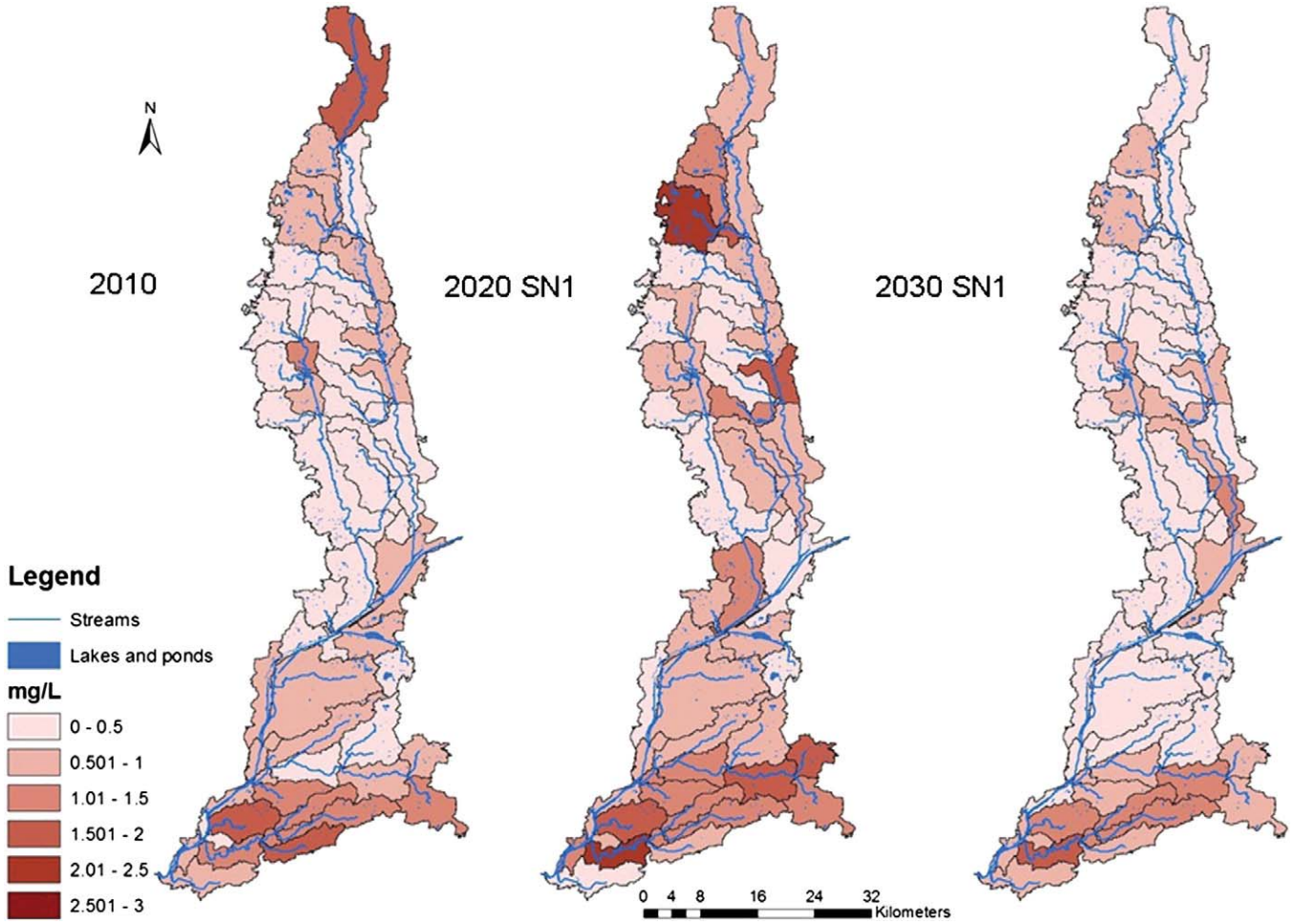

Fig. 17. Total phosphorus concentration for March under SRES A1B climate scenario. Note: SN1 = land use/planning scenario.

of total suspended sediments and phosphorus at both the general watershed and sub-basin scales in the Des Plaines River watershed. Future climate change exerts a larger impact on the concentration of pollutants than the potential impact of land use change. The various land use/planning scenarios demonstrated slight differences between nonpoint source pollutant concentrations under constant climate emission scenario, but this trend significantly veered when inter-seasonal and inter-climate emission types were examined. Considerable levels of late winter and early spring river discharge indicated by SRES A1B would result in lower phosphorus concentration by activating dilution over loading of phosphorus within the watershed. The response of future water quality to climate and land use heavily depends on the type of climate emission scenario being evaluated.

At the sub-basin scale, the growth of middle and high density residential land use at the expense of low density residential would help reduce late winter and early spring loadings and the concentration of total suspended solids. Although it is difficult to prescribe land use configuration that can mitigate elevated levels of phosphorus in the future, our modeling result suggests that increased open space/vegetation and low density residential areas at the expense of industrial, middle density residential, and commercial/urban mix land categories might, to some extent, serve as land use mitigation strategies at the sub-basin scale.

This modeling approach developed in this study can be applied to watersheds in other metropolitan settings provided the data and expertise are available. It would be interesting to assess total suspended solids and phosphorus response to other climate emission scenarios and watersheds that have more abrupt changes in elevation compared to the Des Plaines River watershed. Finally, a longer term analysis of future land and climate changes is recommended to compare possible changes in water quality beyond 2030.

Acknowledgment

This research is sponsored by a NOAA Illinois-Indiana Sea Grant fund (Grant #NA06OAR4170079). The authors wish to thank the anonymous reviewers for their constructive comments and suggestions, which help improve the manuscript.

References

Abbaspour KC. User manual for SWAT-CUP. SWAT calibration and uncertainty analysis programs. [93 pp.]Dubendorf, Switzerland: Ewag: Swiss Fed. Inst. Of Aquat. Sci. and Technol; 2007. [Available at] http://www.eawag.ch/organization/abteilungen/siam/software/swat/index_EN.

Abbaspour KC, Faramarzi M, Ghasemi SS, Yang H. Assessing the impact of climate change on water resources in Iran. Water Resour Res 2009;45:1–16.

Adam JC, Lettenmaier DP. Adjustment of global gridded precipitation for systematic bias. J Geophys Res 2003;108:1–14.

Angel S, Sheppard S, Civco D, Buckley R, Chabaeva A, Gitlin L, et al. The dynamics of global urban expansion. Washington D.C: Department of Transport and Urban Development, The World Bank; 2005.

Arnold JG, Allen PM, Bernhardt G. A comprehensive surface-ground flow model. J Hydrol 1993;142:47–69.

Arnold JG, Srinivasan R, Muttiah RS, Williams JR. Large area hydrologic modeling and assessment part 1: model development. J Am Water Resour Assoc 1998;34(1):73–89.

Asselman NE, Middelkoop H, Dijk PM. The impacts of changes in climate and land use on soil erosion, transportation and deposition of suspended sediment in the River Rhine. Hydrol Processes 2003;17:3225–44.

Beighley RE, Dunne T, Melack JM. Impacts of climate variability and land use alterations on frequency distributions of terrestrial runoff loading to coastal waters in Southern California. J Am Water Resour Assoc 2008;44(1):62–74.
Bekele EG, Knapp V. Watershed modeling to assessing impacts of potential climate change on water supply availability. Water Resour Manage 2010;24:3299–320.
Bradley SB, Lewin J. Transport of heavy metals on suspended sediments under high flow conditions in a mineralized region of Wales. Environ Pollut B Chem Phys 1982;4 (4):257–67.
Chang H. Water quality impacts of climate and land use changes in Southern Pennsylvania. Prof Geographer 2004;56(2):240–57.
Chicago Metropolitan Agency for Planning. Land use inventory (versions 1.0 and 2.1), 2010. Chicago, IL; 2010a.
Chicago Metropolitan Agency for Planning. Go to 2040 comprehensive regional plan. Full version, October 2010, Chicago, IL; 2010b.
Chung E, Park K, Lee KS. The relative impacts of climate change and urbanization on the hydrologic response of a Korean urban watershed. Hydrol Processes 2011;25:544–60.
Clarke KC, Hoppen S, Gaydos L. A self-modifying cellular automaton model of historical urbanization in the San Francisco Bay Area. Environ Plan Plan Design 1997;24: 247–61.
Congalton RGA. A review of assessing the accuracy of classification of remotely sensed data. Remote Sens Environ 1991;37:35–46.
Cutler I. Chicago: metropolis of the mid-continent. 4th edition. Chicago, IL: The Geographic Society of Chicago; 2006.
Duan Q, Gupta VK, Sorooshian S. A shuffle complex evolution approach for effective and efficient global minimization. J Optimiz Theory App 1993;76:501–21.
Ducharne A, Baubion C, Beudoin N, Benoit M, Billen G, Brisson N, et al. Long-term perspective of the Seine River system: confronting climate and direct anthropogenic changes. Sci Total Environ 2007;375:292–311.
Emmerth PP, Bayne DR. Urban influence on phosphorus and sediment loading of West Point Lake, Georgia. J Am Water Resour Assoc 1996;32(1):145–54.
Feddema J, Oleson K, Bonan G, Mearns L, Buja L, Meehl G, et al. The importance of land cover change in simulating future climates. Science 2005;310:1674–8.
Foley J, DeFries R, Asner G, Barford C, Bonan G, Carpenter S, et al. Global consequences of land use. Science 2005;309:570–4.
Freeman W, Fox J. ALAWAT: a spatially allocated watershed model for approximating stream, sediment, and pollutant flows in Hawaii, USA. Environ Manage 1995;19(4): 567–77.
Goonetilleke A, Thomas E, Ginn S, Gilbert D. Understanding the role of land use in urban storm water quality management. J Environ Manage 2005;74(1):31–42.
Hepinstall J, Alberti M, Marzluff J. Predicting land cover change and avian community responses in rapidly urbanizing environments. Landsc Ecol 2008;23:1257–76.
Ierodiaconou D, Laurenson L, Leblanc M, Stagnitti F, Duff G, Salzman S. Multi-temporal land use mapping using remotely sensed techniques and the integration of a pollutant load model in a GIS. In: Chen Y, Takara K, Cluckie I, De Smedt F, editors. GIS and remote sensing in hydrology, water resources and environmentIAHS Publication 209; 2004. p. 343–52.
Imhoff JC, Kittle Jr JL, Gray MR, Johnson TE. Using the Climate Assessment Tool (CAT) in USA EPA BASINS integrated modeling system to assess watershed vulnerability to climate change. Water Sci Technol 2007;56:49–56.
IPCC. Climate change 2001: the scientific basis. In: Houghton JT, Ding Y, Griggs DJ, Noguer M, van der Linden PJ, Dai X, Maskell K, Johnson CA, editors. Contribution of working group 1 to the third assessment report of the intergovernmental panel on climate change. United Kingdom and New York, NY, USA: Cambridge University Press; 2001.
Jensen JR. Introductory digital image processing: a remote sensing perspective. 3 rd edition. NJ: Upper Saddle River; 2005.
Jeppesen E, Kronvang B, Meerhoff M, Sondergaard M, Hansen K, Anderson H, et al. Climate change effects on runoff, catchment phosphorus loading and lake ecological state, and potential adaptations. J Environ Qual 2009;38(5):1930–41.
Kahya O, Bayram B, Reis S. Land cover classification with an expert system approach using Landsat ETM imagery: a case study of Trabzon. Environ Monit Assess 2010;160:431–8.
Krause P, Boyle DP, Base F. Comparison of different efficiency criteria for hydrological model assessment. Adv Geosci 2005;5:89–97.
Labs Clark. IDRISI Taiga: land change modeler software for ArcGIS. Worcester, MA: Clark University; 2009.
Landis JD. The California urban futures model: a new generation of metropolitan simulation models. Environ Plan B Plan Design 1993;21:399–420.
Landis JD. Imagining land use futures: applying the California futures model. J Am Plann Assoc 1995;61(4):438–57.
Lawrence RL, Wright A. Rule-based classification systems using classification and regression tree (CART) analysis. Photogramm Eng Remote Sens 2001;67(10): 1137–42.
Lee RG, Flamm R, Turner MG, Bledsoe C, Chandler P, DeFerrari C, et al. Integrating sustainable development and environmental vitality, a landscape ecology approach. In: Naiman RJ, editor. Watershed management: balancing sustainability and environmental change. New York, NY: Springer-Verlag; 1992. p. 499–521.
Lindgren A. Dagvattenbelastning på sjöar och vattendrag i förhållande till andra föroreningskällor (The influence of stormwater on lakes and watercourses in comparison to other pollutant sources). Publication 2001:114. Swedish Road administration; 2001 [In Swedish].
Loomis J. Integrated public lands management: principles and applications to national forests, parks and wildlife refuges, and BLM lands. 2nd ed. New York: Columbia University Press; 2002.
Lopez E, Bocco G, Mendoza M, Duhau E. Predicting land cover and land use change in the urban fringe: a case in Morelia city, Mexico. Landscape Urban Plann 2001;55 (4):271–85.
Lu D, Mausel P, Brondizio E, Moran E. Assessment of atmospheric correction methods for Landsat TM data applicable to Amazon basin LBA research. Int J Remote Sens 2002;23(13):2651–71.
Maestas JD, Knight RL, Gilgert WC. Biodiversity across a rural land-use gradient. Conserv Biol 2003;17(5):1425–34.
Maurer EP, Adam JC, Wood AW. Climate model based consensus on the hydrological impacts of climate change to the Rio Lempa basin of Central America. Hydrol Earth Syst Sci 2009;13:183–94.
Maximov, I.A. Integrated assessment of climate and land use change effects on hydrology and water quality of the Upper and Lower Great Miami River. PhD dissertation, Department of Geography, University of Cincinnati; 2003.
Meehl GA, Covey C, Delworth T, Latif M, McAvaney B, Mitchell JF, et al. The WCRP CMIP3 multi-model dataset: a new era in climate change research. Bull Am Meteorol Soc 2007;88:1383–94.
NASA. Panoply version 2.9.2 user guide. New York, N.Y: Goddard Institute for Space Studies; 2010.
Nash JE, Sutcliffe JV. River flow forecasting through conceptual models: part 1 — a discussion of principles. J Hydrol 1970;10(3):282–90.
Neitsch SL, Arnold JG, Kiniry JR, Srinivasan R, Williams JR. Soil and Water Assessment Tool input/output file documentation; 2004.
Parks RJ. Models of forested and agricultural landscapes: integrating Economics. In: Turner MG, Gardner RH, editors. Quantitative methods in landscape ecology: the analysis and interpretation of landscape heterogeneity. New York, NY: Springer-Verlag; 1991. p. 309–22.
Petit C, Scudder T, Lambin E. Quantifying processes of land-cover change by remote sensing: resettlement and rapid land-cover change in southeastern Zambia. Int J Remote Sens 2001;22(17):3435–56.
Pijanowski BC, Brown DG, Shellito BA, Manik GA. Using neural networks and GIS to forecast land use changes: a land transformation model. Comput Environ Urban Syst 2002a;26(6):553–75.
Pijanowski BC, Shellito B, Pithadia S, Alexandridis K. Forecasting and assessing the impact of urban sprawl in coastal watersheds along eastern Lake Michigan. Lakes Reserv Res Manage 2002b;7:271–85.
Praskievicz S, Chang H. Impacts of climate change and urban development on water resources in the Tualatin River Basin, Oregon. Ann Assoc Am Geogr 2011;101(2): 249–71.
Qian B, Gameda S, Hayhoe H. Performance of stochastic weather generators LARS-WG and AAFC-WG for reproducing daily extremes of diverse. Can clims Clim Res 2008;37:17–33.
Qu W, Kelderman P. Heavy metal contents in the Delft canal sediments and suspended solids of the River Rhine: multivariate analysis for source tracing. Chemosphere 2001;45(6–7):919–25.
Rounsevell MD, Reginster I, Araujo MB, Carter TR, Dendoncker N, Ewert F, et al. A coherent set of future land use change scenarios for Europe. Agr Ecosyst Environ 2006;114:57–68.
Sala O, Chapin F, Armesto J, et al. Global biodiversity scenarios for the year 2100. Science 2000;287:5459-1770.
Soranno PA, Hubler SL, Carpenter SR. Phosphorus loads to surface waters: a simple model to account for spatial pattern of land use. Ecol Appl 1996;6(3):865–78.
Stone MC, Hotchkiss RH, Hubbard CM, Fontaine TA, Mearns LO, Arnold JG. Impacts of climate change on Missouri River basin water yield. J Am Water Resour Assoc 2001;37(5):1119–29.
Theobald D, Hobbs N. Forecasting rural land-use change: a comparison of regression- and spatial transition-based models. Geograp Environ Model 1998;2(1):65–82.
Theobald D, Hobbs N. A framework for evaluating land use planning alternatives: protecting biodiversity on private land. Conserv Ecol 2002;6(1):5. http://www.consecol.org/vol6/iss1/art5.
Tu J. Combined impact of climate and land use changes on streamflow and water quality in eastern Massachusetts, USA. J Hydrol 2009;379:268–83.
Turner MG. Spatial simulation of landscape change in Georgia: a comparison of 3 transition models. Landsc Ecol 1987;1:29–36.
USEPA. Our built and natural environments: a technical review of the interactions between land use, transportation, and environmental quality. EPA 231-R-01-002; 2001.
Van Griensven A. Sensitivity, auto-calibration, and model evaluation in SWAT 2009. User guide distributed with ArcSWAT program; 2005.
Veith TL, Ghebremichael LT. How to: applying and interpreting the SWAT auto-calibration tools. 2009 International SWAT conference proceedings, August 5–7, 2009, University of Colorado at Boulder, Boulder Colorado. Texas Water Resources Institute Technical Report No. 356Texas A&M University System; 2009. p. 26–33.
Walling DE, Webb BW. Chapter 3: water quality. 1: physical characteristics. In: Calow P, Pettse GE, editors. The rivers handbook, Vol. 1. Oxford: Blackwell; 1992. p. 48–72.
Waschbusch RJ, Selbig WR, Bannerman RT. Sources of phosphorus in stormwater and street dirt from two urban residential basins in Madison, Wisconsin, 1994–1995. U.S. Geological Survey, Water Resources Investigations Report; 1999. p. 99–4021.
Weng Q. Modeling urban growth effects on surface runoff with the integration of Remote Sensing and GIS. Environ Manage 2001;28(6):737–48.
Weng Q. Land use change analysis in the Zhujiang Delta of China using satellite remote sensing, GIS, and stochastic modeling. J Environ Manage 2002;64(3):273–84.
Wentz EA, Nelson D, Rahman A, Stefanov WL, Roy SS. Expert system classification of urban land use/land cover for Delhi, India. Int J Remote Sens 2008;29(15):4405–27.
Wilby RL, Charles SP, Zorita E, Timbal B, Whetton P, Mearns LO. Guidelines for use of climate scenarios developed from statistical downscaling methods [online] Available from the DDC of IPCC TGCIA. http://www.ipccdata.org/guidelines/dgm_no2_v1_09_2004.pdf2004.
Wilks DS. Use of stochastic weather generators for precipitation downscaling. Wiley Interdiscip Rev Clim Change 2010;1(6):898–907.

Willmott CJ. On the validation of models. Phys Geograp 1981;2:184–94.
Wilson CO, Weng Q. Assessing surface water quality and its relations with urban land cover changes in the Lake Calumet Area, Greater Chicago. Environ Manage 2010;45:1096–111.
Winter JG, Duthie HC. Export coefficient modeling to assess phosphorus loading in an urban watershed. J Am Water Resour Assoc 2000;36(5):1053–61.
Wood AW, Leung LR, Sridhar V, Lettenmeier DP. Hydrological implications of dynamical and statistical approaches to downscaling climate model outputs. Clim Change 2004;62:189–216.
Wu Q, Li H, Wang R, Paulussen J, He Y, Wang M, et al. Monitoring and predicting land use change in Beijing using remote sensing and GIS. Landscape Urban Plann 2006;78:322–33.
Yang J, Reichert P, Abbaspour KC, Yang H. Comparing uncertainty analysis techniques for SWAT application to Chaohe Basin in China. J Hydrol 2008;358:1–23.
Young WJ, Marston FM, Davis JR. Nutrient export and land-use in Australian Catchments. J Environ Manage 1996;47:165–83.
Yusop Z, Tan LW, Ujang Z, Mohamed M, Nasir KA. Runoff quality and pollution loadings from a tropical urban catchment. Water Sci Technol 2005;52(9):125–32.
Zhang C, Li W. Markov chain modeling of multinomial land-cover classes. Sci Remote Sens 2005;42:1–18.
Zhang X, Srinivasan R, Hao F. Predicting hydrologic response to climate change in the Louhe River basin using the SWAT model. Am Soc Agri Biol Eng 2007;50(3):901–10.
Zhou G, Liebhold AM. Forecasting the spatial dynamics of gypsy moth outbreaks using cellular transition models. Landsc Ecol 1995;10:177–89.
Zonta R, Collavini F, Zaggia L, Zuliani A. The effect of floods on the transport of suspended sediments and contaminants: a case study from the estuary of the Dese River (Venice Lagoon, Italy). Environ Int 2005;31(7):948–58.